The 2008 Kersten Lecture
Integration of geotechnical and structural design in tunneling

Evert Hoek
Consulting Engineer, Vancouver, British Columbia, Canada

Carlos Carranza-Torres
CCT Rock Engineering, Minneapolis, Minnesota USA

Mark Diederichs
Geological Sciences and Geological Engineering, Queen's University, Kingston, Ontario, Canada

Brent Corkum
Rocscience Inc., Toronto, Canada

The 2008 Kersten Lecture
Integration of geotechnical and structural design in tunneling

Evert Hoek
Consulting Engineer, Vancouver, British Columbia, Canada

Carlos Carranza-Torres
CCT Rock Engineering, Minneapolis, Minnesota USA

Mark Diederichs
Geological Sciences and Geological Engineering, Queen's University, Kingston, Ontario, Canada

Brent Corkum
Rocscience Inc., Toronto, Canada

ABSTRACT: In the majority of modern rock tunnels the deformation and hence the stability of the tunnel is controlled by a combination of reinforcement and support systems. The reinforcement consists of rockbolts or cables which modify the properties of the rock mass in much the same way as reinforcement does in concrete. The support systems generally involve steel sets or lattice girders fully embedded in shotcrete and these provide resistance to control the convergence of the tunnel. This paper describes the methods that can be used to optimize the design of tunnels using a combination of reinforcement and support methods. Particular attention is given to tunnels in very weak rock or soil in which large deformations can occur. Two case histories are presented to illustrate the integration of geotechnical and structural design methods. The first is a 12 m span two lane highway tunnel, excavated by top heading and benching in a very weak rock mass and the second involves a 25 km long, 5.5 m diameter water supply tunnel through the Andes in Venezuela.

1 INTRODUCTION

Current practice in tunnel reinforcement and lining design tends to vary a great deal, depending upon national or owner imposed design requirements, local tradition and practice and the experience of the tunnel designer. There are no universally accepted guidelines on how to assess the safety of a tunnel or the acceptability of a design and this means that engineering judgment and experience play a very large role in the design of tunnel reinforcement and linings.

There is a general desire to define a factor of safety for tunnel design but this has proved to be an extremely difficult task and there are very few methods that are considered acceptable. One of these methods, described by Kaiser (1985), and Sauer et al (1994), involves the use of support capacity diagrams and, indeed, there are a few tunnel design companies that use this methodology. However, the available papers are generally lacking in detail and there is no mention of this method in design guidelines such as the Tunnel Lining Design Guide published by the British Tunnelling Society (2004). Consequently, the average tunnel designer is left with few options other than the use of tunnel classification systems (Barton et al, 1974, Bieniawski, 1973), gener-

al empirical guidelines and the advice of experienced tunnel consultants. The main difficulty with this approach is to decide when the design is acceptable (Hoek, 1992).

In an effort to remedy some of these problems, the authors have set out to present two relatively complex case histories in sufficient detail that tunnel designers can follow the use of support capacity diagrams as a tunnel design tool. Based on a paper by Carranza-Torres and Diederichs (2009), the derivation of the equations used to define these support capacity curves are presented in an appendix and it is relatively simple to program these equations in a spreadsheet.

The support capacity diagrams presented in this paper are based on elastic analyses and the authors recognize that this is a simplification compared to much more sophisticated non-linear models that are used in structural engineering. However, given the uncertainties associated with the loads imposed on tunnel linings, this simplification is considered to be justified. These loads depend upon the adequacy of the geological model, the properties of the rock mass surrounding the tunnel, the in situ stresses and the groundwater conditions. All of these contributing factors are open to a wide range of interpretations, particularly during the design stages in a tunnelling project. Consequently, the aim in developing the elastic support capacity diagrams presented in this paper is to provide the tunnel designer with a set of tools of comparable accuracy to the input data.

2 CASE HISTORY 1 – A SHALLOW TUNNEL AND ADJACENT OPEN CUT

This case history, assembled from a number of actual tunnel designs, involves a 12 m span highway tunnel excavated by drill and blast methods using a top heading and bench approach. Once the tunnel has been excavated and a final concrete lining has been cast in place, an open cut is excavated close to and downhill from the tunnel to accommodate a second carriageway.

The overall geometry of the slope, the tunnel and the adjacent cut is shown in Figure 1. The rock mass is a gently dipping interbedded sedimentary sequence of jointed sandstone, bedded sandstone and a series of shear zones parallel to bedding. The properties of the individual rock units, based on a nearby tunnel in a similar rock mass, are listed in Table 1 and the corresponding Mohr envelopes are plotted in Figure 2.
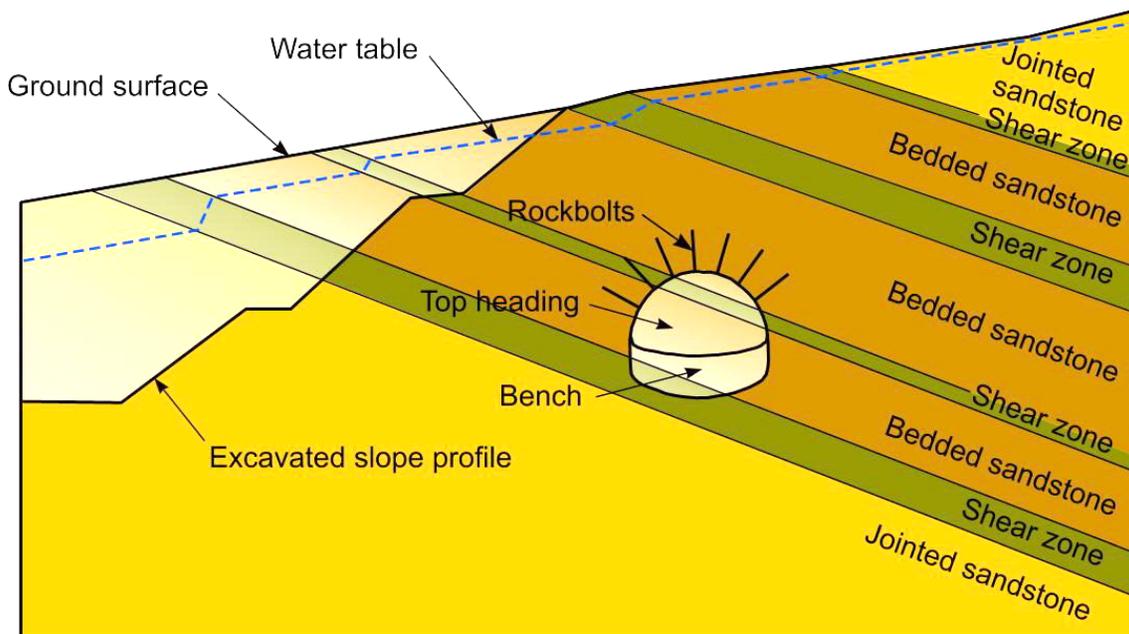

Figure 1. Geometry of the original slope showing the rock layers, the location and geometry of the tunnel and slope excavations and the original water table.

Table 1. Rock mass properties

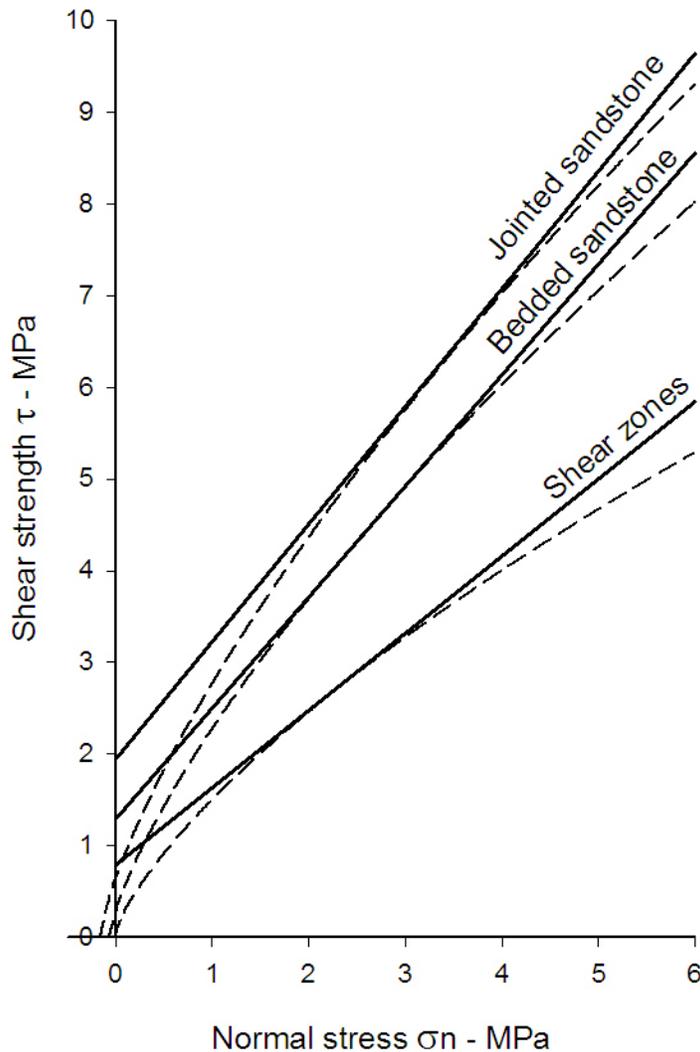| Property	Jointed sandstone		Bedded sandstone		Shear zones	
	Peak	Residual	Peak	Residual	Peak	Residual
Cohesive strength c - MPa	2.0	1.5	1.4	1.2	0.8	0.8
Friction angle ϕ - degrees	52	50	50	47	40	40
Rock mass modulus E - MPa	9500		4000		650	
Poisson's ratio	0.25		0.25		0.3	
Permeability – m/sec	1×10^{-6}		1×10^{-6}		1×10^{-7}	

Figure 2. Mohr failure envelopes for individual rock units.

Note that the friction angles shown in Table 1 may appear to be unusually high, particularly to soil mechanics readers. This is because the tunnel is very shallow and the average confining stress in the rock mass surrounding the tunnel is only about 1 MPa. Under these conditions the Mohr failure envelopes are strongly curved, as shown by the dashed lines in Figure 2 (Hoek et al, 2002) and the Mohr Coulomb parameters are estimated from tangents to the curved envelopes.

2.1 *In situ stress conditions*

The vertical stress acting on the rock mass in which this tunnel will be excavated is given by the product of the depth below surface and the unit weight of the rock. Horizontal stress magnitudes and directions can vary greatly, depending upon the tectonic history of the area, the variation in stiffness of different rock units in the rock mass and the local topography. As a starting point for this analysis it has been assumed that the ratio of vertical to horizontal stresses parallel to the tunnel axis is 2:1 and that the ratio normal to the tunnel axis is 1.5:1.

If no in situ stress measurements are available in the vicinity of the tunnel then it is prudent for the tunnel designer to check the sensitivity of the design to variations in these ratios between 0.5:1 and 2:1. If the design proves to be sensitive to horizontal stress variations then steps should be taken to have in situ stress measurements made before the design proceeds to completion. An alternative is to leave sufficient flexibility in the contract to allow design changes during construction and to rely on the back analysis of tunnel convergence measurements to determine the in situ stresses acting on the tunnel.

2.2 *Groundwater conditions*

The excavation of the tunnel and the slope for the adjacent carriageway result in changes in the groundwater conditions in the slope. These changes have a significant impact on the effective stresses in the rock mass surrounding the tunnel. Consequently, a full analysis of these groundwater conditions is a starting point for this analysis of the tunnel stability.

Assuming a permeability of 1×10^{-7} m/sec for the shear zones and 1×10^{-6} m/sec for the jointed and bedded sandstones (see Table 1), a finite element analysis of the groundwater conditions in the slope was carried out. The resulting water tables, for different stages of tunnel and slope excavation, are shown in Figure 3. In this analysis it was assumed that the tunnel acts as a drain except for an extreme long term condition in which the tunnel drains are blocked.

In the finite element analysis of the tunnel lining that follows the pore water pressures and the resulting effective stresses, from the groundwater analysis described above, have been incorporated into the tunnel stability model.
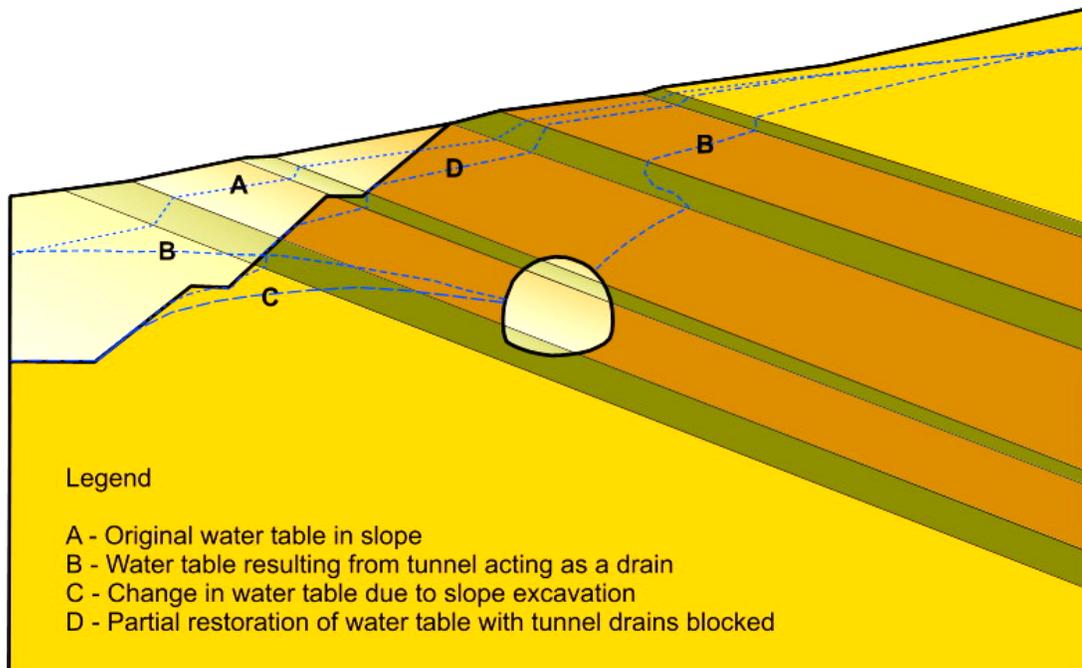

Legend

A - Original water table in slope
B - Water table resulting from tunnel acting as a drain
C - Change in water table due to slope excavation
D - Partial restoration of water table with tunnel drains blocked

Figure 3. Water tables at different stages of tunnel and slope excavation and assuming long term blockage of the tunnel drains.

2.3 *Lining requirements*

The client's requirements for the lining of the tunnel are as follows:

1. An initial lining consisting of steel sets or lattice girders embedded in shotcrete, with the addition of rockbolts if required, sufficient to stabilize the tunnel during construction and until the final lining is placed.
2. A drainage layer consisting of porous geotextile fabric, connected to drainage pipes in the final tunnel invert.
3. A waterproof membrane to prevent water entering into the space behind the final concrete lining.
4. A cast in place concrete lining and invert capable of resisting loads imposed by the surrounding rock mass for both short and long term operation of the tunnel. The factor of safety of the final reinforced concrete lining should exceed 2.0 for normal operating loads and 1.5 for unusual and long term loads.

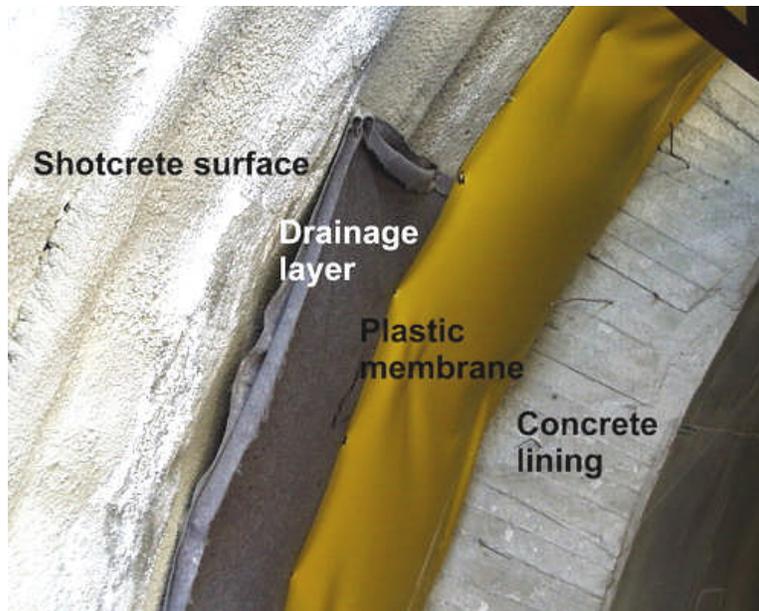A typical tunnel lining, designed to meet such requirements, is illustrated in Figure 4.

Figure 4. Construction of a complete tunnel lining consisting of an initial lining of lattice girders embedded in shotcrete, a geotextile drainage layer, a waterproof plastic membrane and a cast-in-place concrete final lining.

2.4 *Top heading versus full face excavation*

An important issue that has to be considered by any drill and blast tunnel designer is whether to specify excavation of the tunnel using a top heading and bench approach or a full face excavation method. Small diameter tunnels, less than say 6 m span, are invariably driven by full face methods since stabilization of the face, if required, is relatively simple. At the other end of the spectrum, large underground caverns are almost always excavated in multiple stages from a top heading or from side drifts. The 12 m span transportation tunnel considered in this example falls in the range where either top heading and bench or full face excavation can be used. Full face excavation has many advantages in terms of geometrical simplicity and, in ground of adequate strength, greater rates of tunnel excavation. Consequently, where possible it is the preferred method of tunneling.

One of the technical factors that controls the choice of which method to use is the stability of the tunnel face. When the stresses in the rock mass surrounding a tunnel exceed the strength of the rock mass a zone of failure or a "plastic" zone is formed around the tunnel. As shown in the derivation of longitudinal displacement profiles for tunnels in Appendix 1, when the radius of the plastic zone around a tunnel exceeds twice the radius of the tunnel, the zone of failure around the tunnel interacts with the failed rock ahead of the tunnel face to form a continuous bullet shaped plastic zone. This three-dimensional plastic zone becomes increasingly difficult to stabilize as the ratio of stress to available rock mass strength increases.

Stabilizing the plastic zone ahead of the tunnel face is generally achieved by means of fully grouted fiberglass dowels parallel to the tunnel axis. The reason for using fiberglass dowels is that they can be cut off as the tunnel advances and they do not damage conveyor belts in the muck disposal system. These dowels are typically placed in a grid pattern of 1 m x 1 m and their total length is approximately equal to the span of the tunnel. For 12 m long dowels an overlap of 3 to 4 m is generally used to ensure that there is continuous support of the face.

Lunardi (2000) discusses the action of face reinforcement in considerable detail and the authors have no disagreement with his statement that ".... In order to prevent instability of the face, and therefore the cavity (tunnel), preconditioning measures must be adopted, appropriately balanced between the face and the cavity, of an intensity adequate to the actual stress conditions relative to the strength and deformation properties of the medium". The preconditioning to which he refers includes the placement of fiberglass dowels, forepoles and other devices that control the deformation of the rock mass ahead of the tunnel face. Achieving an appropriate balance between the face and the tunnel cavity requires a three dimensional analysis of the bullet shaped plastic zone discussed above.

In addition to the stability of the face, consideration has also to be given to the deformations that control the stability of the tunnel itself. Depending upon the in situ stress field and the characteristics of the rock mass surrounding the tunnel, these deformations may be more important than those in the rock ahead of the face. In such cases, the control of the tunnel deformations will determine the choice between top heading and bench and full face excavation.

Practical considerations related to the size of the tunnel, availability of specialized equipment required for the installation of pre-reinforcement, local contracting experience and the preference of the owner can also play an important role in choosing between top heading and bench and full face excavation methods.

In the tunnel under consideration in this model (Figure 1), the owner considered that the risk of losing control of the face due to the presence of the weak shear zones is unacceptably high. Consequently the use of a top heading and bench approach has been specified, in spite of the fact that it may have been possible to drive this tunnel by full face excavation.

2.5 *Analysis of face stability*

The analysis of the stability of a top heading or a full face tunnel face requires a three dimensional analysis. In simple cases this can be done by means of an axi-symmetric application of a two-dimensional numerical analysis (see Figure A1.3 in Appendix 1). In more complex cases, such as that under consideration in this example, a full three-dimensional analysis is required.

The purpose of the three-dimensional analysis is to simulate in the most realistic possible way the mechanical process of excavation and support and reinforcement installation behind the face and, if applicable, on the face itself to investigate whether the face shows signs of instability. In these three-dimensional models, face instability normally manifests itself as caving of the face resulting in a plastic failure zone that extends ahead of the face or, if the tunnel is relatively shallow as in this example, towards the ground surface. Excessively large displacements can occur and the numerical model tends not to converge (i.e., reach an asymptotic value) as the excavation sequence progresses.

Figure 5 shows the three-dimensional numerical model used to analyze the stability of the face in this example. Note that only half of the model, as defined by a vertical plane cutting through the tunnel axis, is represented in this figure. The model considers excavation of the top heading through the interbedded sedimentary sequence introduced in Figure 1. Mechanical properties of the different rock types are those indicated in Figure 2 and Table 1. The in situ

stress conditions prior to excavation assumed for the model are those discussed in Section 2.1, while the groundwater conditions correspond to the worst case scenario, that of the original water table (configuration A) in Figure 3.

As indicated in Figure 5, the three-dimensional model simulates the mechanical process of advancing the top heading in increments of 2 meters, corresponding to the design blast round length of 2 m, and installing shotcrete and rockbolts at a distance of 2 meters behind the face, corresponding to the design length of installation of support and reinforcement behind the face. The geometrical and mechanical characteristics of the support and reinforcement used are the same considered in the two-dimensional numerical analyses to be discussed in later sections. In addition, the model simulates the process of installation of a set of 60 fiberglass dowels in a circumferential pattern at the face, with an approximate spacing of 1 meter between dowel heads. In this case, the dowels are installed at intervals of 8 meters on the face, leading to a minimum overlap length of 4 meters between two sets of dowels. The geometrical and mechanical properties of fiberglass dowels are normally provided by the manufacturer; this example considers dowels of 18 mm diameter, with a Young's modulus of 40,000 MPa and a tensile strength of 1000 MPa.
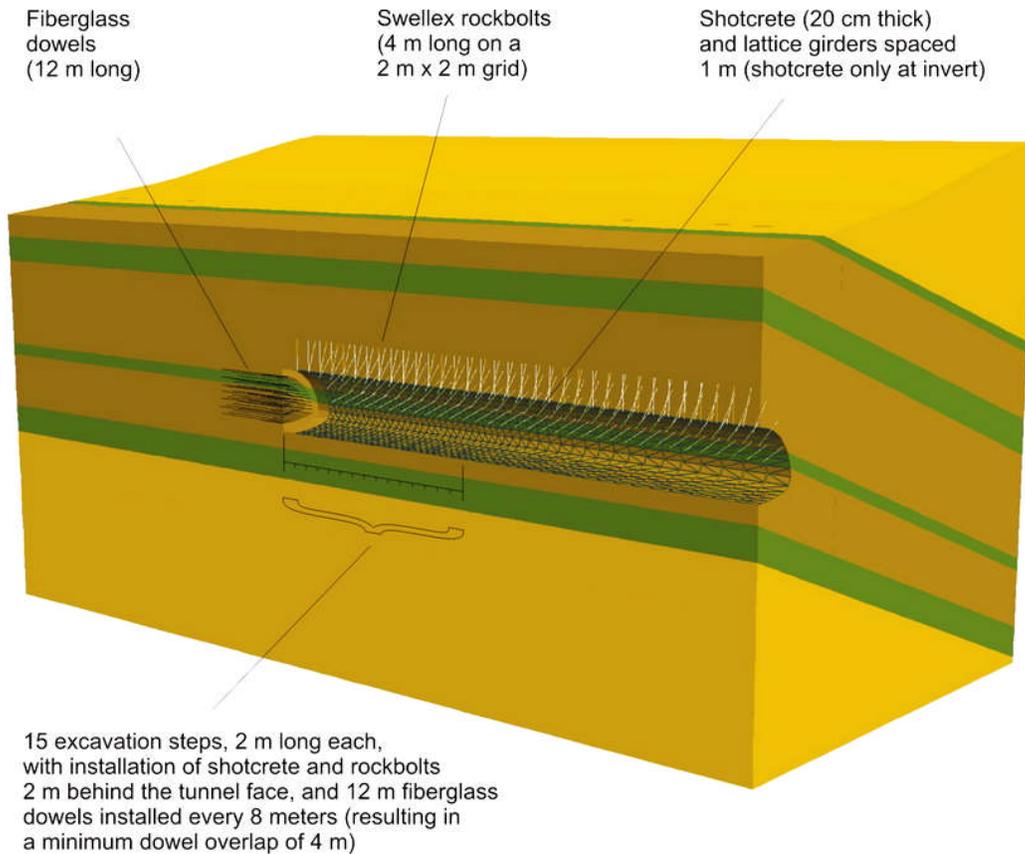

Figure 5. View of the three-dimensional numerical model used to analyze stability of the tunnel face.

A total of 15 excavation stages have been considered in this example leading to a total length of sequential advance of 30 meters. For the last stage (indicated in Figure 5) the stability conditions at the face have been inspected. Figure 6 represents contours of resulting magnitude of dis-

placements at this stage. Displacements at the face are below one millimeter. The resulting plastic failure zone is also of limited extent of less than 50 centimeters and does not show any tendency to develop into a caving zone towards the ground surface. Comparison of equivalent results from a model without fiberglass dowels installed at the face reveals that these dowels do indeed make a mechanical contribution to the stability of the tunnel face. Both the extent of plastic zone and resulting displacements at the face, when no fiberglass dowels are considered, are at least twice the values shown in Figure 6.

It is doubtful whether fiberglass dowel reinforcement is actually required in this example and it is probable that the top heading could be advanced safely without reinforcement or with a simpler restraint in the form of a face buttress (Hoek, 2001). However, the calculations presented in Figures 5 and 6 demonstrate the procedure that can be used to analyze the need for face reinforcement and the stabilization that can be achieved by the installation of such reinforcement.
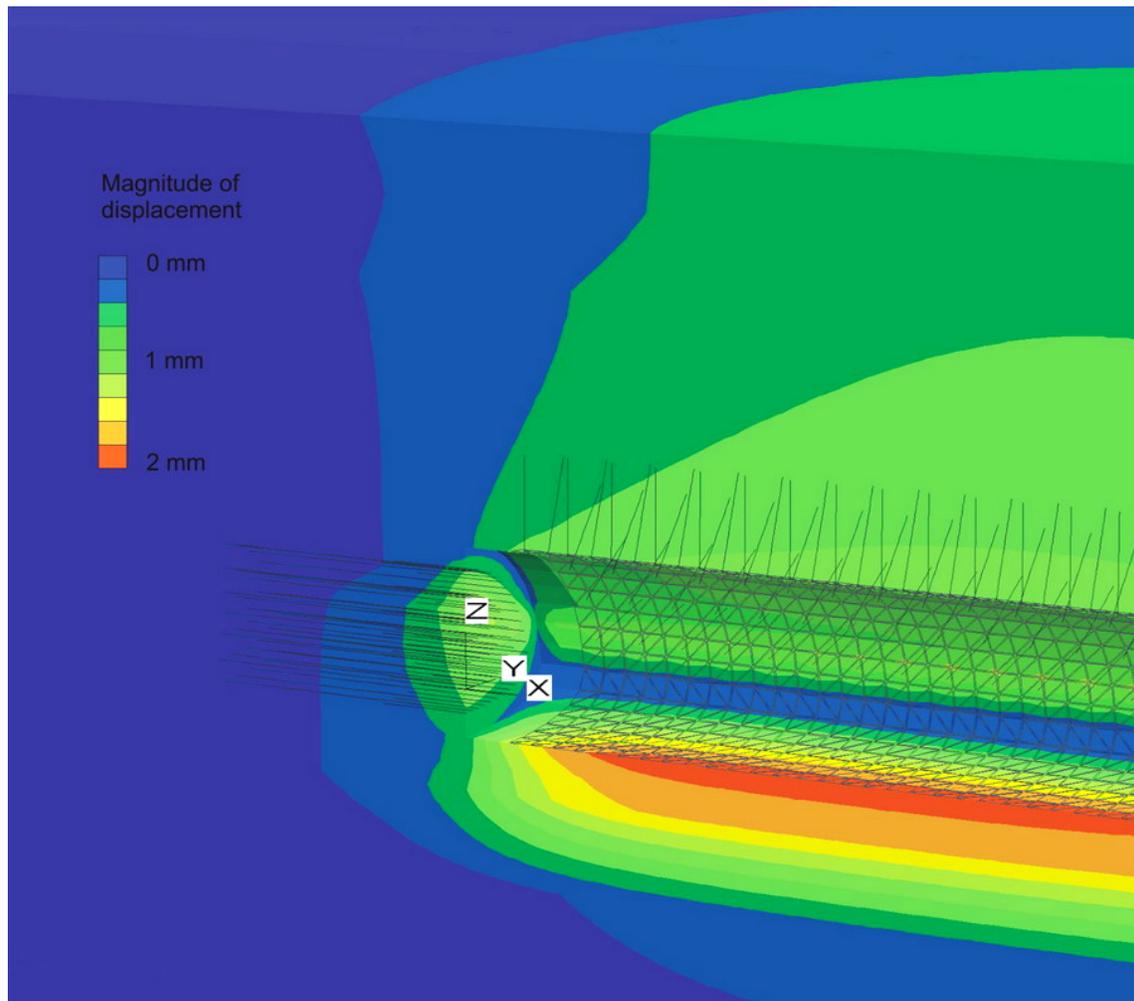

Figure 6. Representation of contours of magnitude of displacements for the last stage of excavation in the three-dimensional model of Figure 5.

2.6 *Characteristic curve and longitudinal deformation profile*

The next step in the design procedure is to determine the point at which the support in the tunnel is installed and activated. In a 12 m span tunnel this would normally be at a distance of between 2 and 4 m behind the face and a distance of 2 m has been chosen for this analysis.

In using a two dimensional analysis of the rock-support interaction it is necessary to simulate the three-dimensional tunnel advance by means of some deformation control process. This means that the deformation that takes place at a distance of 2 m behind the face must be known and controlled to allow the support to be installed and activated. This can be done by calculating the characteristic curve for the rock mass surrounding the tunnel by progressively reducing either an internal support pressure or by progressively decreasing the deformation modulus of an inclusion in the tunnel. In complex situations, such as that under consideration here, the modulus reduction method is preferred since it automatically accommodates variations in the surrounding stress field due to a non-circular tunnel shape and progressive failure in the rock mass as the tunnel deforms.

Figure 7 shows the characteristic curve for this tunnel and the stepwise reduction of the modulus of the inclusion in the tunnel. The analysis required to generate the characteristic curve also shows the extent of failure around the tunnel and this is important in calculating the longitudinal deformation profile in the next stage of the analysis.
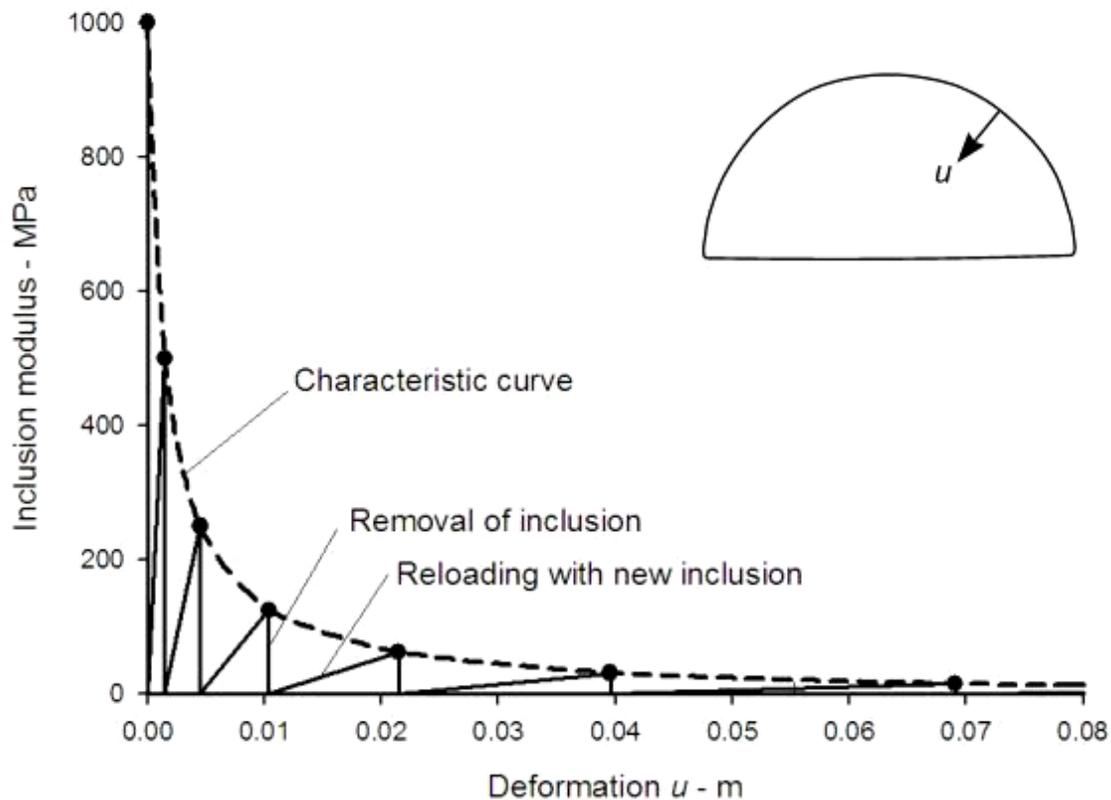

Figure 7. Characteristic curve for the unsupported, undrained tunnel excavated by a full face method. Note that any monitoring point can be chosen on the tunnel boundary since, although the magnitude of the deformations will vary, the shape of the excavation curve will remain constant.
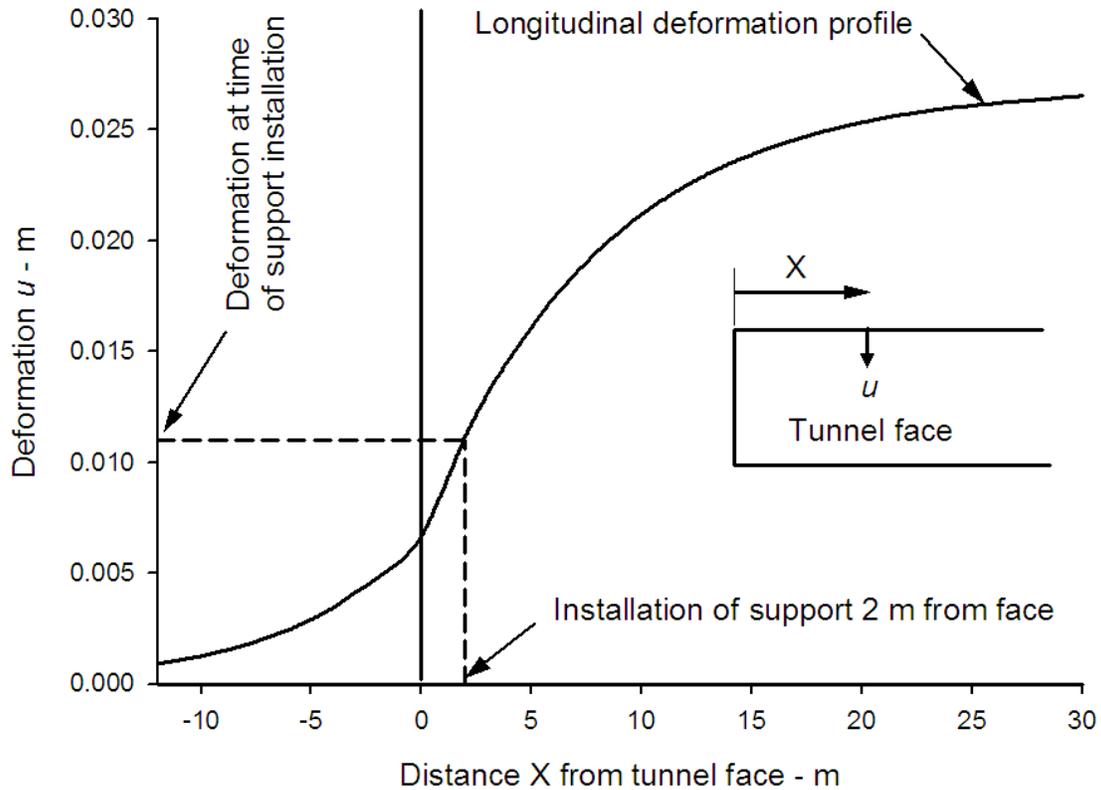
9

Figure 8. Longitudinal deformation profile for a 12 m span tunnel where the radius of the plastic zone is less than twice the radius of the tunnel.

Figure 8 gives a plot for the longitudinal deformation profile for the tunnel in this example. As shown in Appendix 1, this profile depends upon the ratio of the radius of the plastic zone to the radius of the tunnel and, for this example, this ratio is approximately 2:1. Figure A1.5 in Appendix 1 shows that the tunnel closure at the face is approximately one quarter of the final closure at many meters behind the face. The deformation profiles are calculated from equations A1.6 and A1.7.

From Figure 8 it can be seen that installation and activation of the support at a distance of 2 m behind the advancing face corresponds to a deformation of 0.011 m. Using this value in Figure 7, the modulus of the inclusion required to limit the tunnel deformation to this value is approximately 100 MPa. Hence, in constructing the two dimensional model to simulate the three-dimensional effects of the advancing face, an inclusion with a modulus of 100 MPa has been used for the first stage of the calculation. Excavation of this inclusion activates the installed support system and allows it to react to the additional deformation that occurs as the tunnel advances.

2.7 *Analysis of top heading with a flat floor*

For large span tunnels the top heading shape preferred by contractors is illustrated in Figure 9. This consists of an arched roof and a flat floor. The flat floor is simple to excavate and it provides an excellent road base for construction traffic. In good rock at low to moderate stress levels, this top heading shape is acceptable. The suitability of this top heading profile for this example is investigated below.

10

Figure 9. A simple top heading shape in good quality interbedded sandstones and siltstones. The tunnel arch is supported by means of rockbolts and a layer of shotcrete and no face support is required. The flat floor requires no special treatment other than good drainage of surface water accumulations.
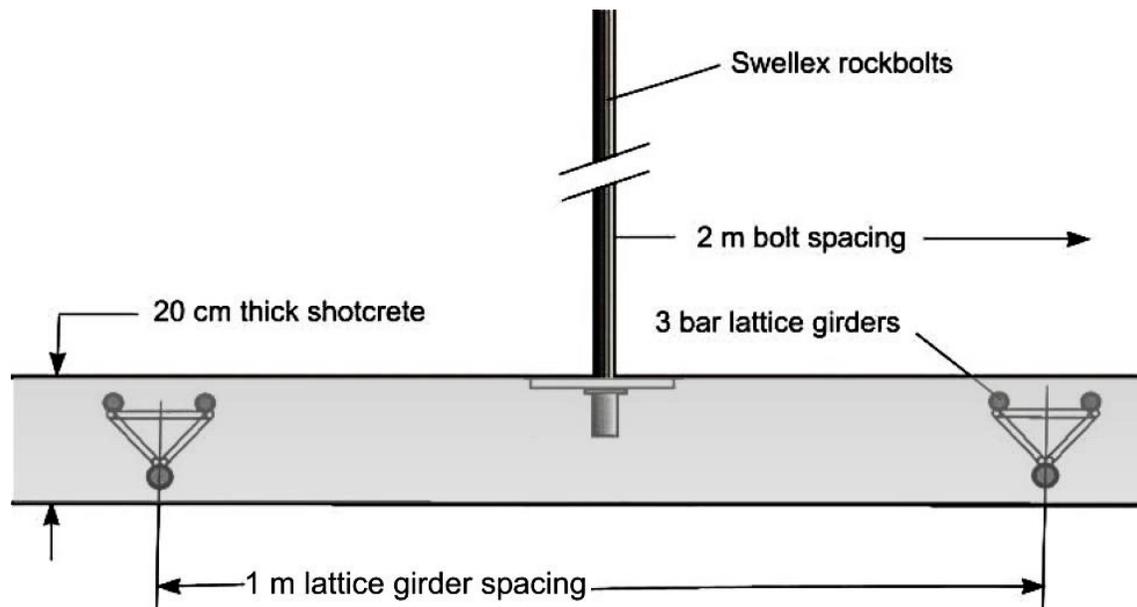

Figure 10. Reinforcement and support for the top heading arch consisting of standard Swellex rockbolts on a 2 m x 2 m grid and 3 bar lattice girders spaced at 1 m centers and embedded in a 20 cm thick shotcrete lining (Not to scale).

Figure 10 gives a cross section through a typical support system used for the initial support of a large span tunnel. This consists of 3 bar lattice girders embedded in a 20 cm thick shotcrete layer. The lattice girders are spaced at 1 m intervals along the tunnel and rockbolts are installed between every second girder at a spacing of 2 m. In this case the rockbolts are 4 m long standard Swellex bolts on a 2 m x 2 m grid spacing.

An important issue that has to be considered in the design of this support system is the time-dependent properties of the shotcrete layer. As described above, the support system is installed 2 m behind the face and activated immediately. The rockbolts and lattice girders respond to the deformation of the rock mass surrounding the tunnel as soon as the tunnel advances but the shotcrete is only 1 day old at this stage and it has not yet developed its full capacity. While it does not carry its full share of the load, because its stiffness is low, this load may be sufficient to induce failure in the shotcrete.

Choosing the shotcrete properties is not quite as simple as one would think. Many tunnel designers turn to structural codes such as the American Concrete Code (ACI 318 - Building Code and Commentary) and follow the recommendations set out in these documents. However, in their Guidelines for Tunnel Lining Design the Technical Committee on Tunnel Lining Design of the Underground Technology Research Council states the following:

"Structural codes should be used with caution. Most codes have been written for above ground structures on the basis of assumptions that do not consider ground-lining interaction. Accordingly, the blind application of structural design codes is likely to produce limits on the capacity of linings that are not warranted in the light of the substantial contributions from the ground and the important influence of construction method on both the capacity and cost of linings.

Specific load factors are not recommended in these guidelines. The loading conditions should be evaluated by a careful, systematic review of the geologic and construction influences. It is important that the evaluation of ground loads and structural details be coordinated to select a factor of safety."

In the support capacity calculations given in this paper the authors have adopted a policy of using the ultimate uniaxial compressive and tensile strengths of shotcrete and concrete and calculating a range of factors of safety. This eliminates the complication of hidden or unknown load factors or safety factors and, by including a family of factor of safety plots in the support capacity diagrams, the user is presented with a clear picture of performance of the lining being designed.

Melbye and Garshol (2000) give shotcrete mix designs and uniaxial strength results, many from in situ cores, for 35 tunneling projects around the world. These results are plotted in Figure 11 and it can be seen that the 28 day strength varies from 25 to 86 MPa. This variation depends upon the mix design, whether the wet or dry shotcrete method was used, whether the shotcrete was applied manually or by robot and upon local factors such as haulage distance between the batch plant and the face. It is the responsibility of the tunnel designer to discuss all of these issues with the shotcrete supplier in order to determine the optimum shotcrete product for a particular site.

For the model under consideration the sequence of loading and the corresponding shotcrete properties are defined in Figure 12 and Table 2 in which the age dependent properties have been assembled from a number of tunnel case histories. In constructing the numerical model used to analyze this case these properties have been incorporated into the shotcrete lining at the stages of excavation shown.

In the case of the top heading with an unsupported and unreinforced flat floor, as illustrated in Figure 13, the heave of the floor induces bending in the lower parts of the lining arch. These bending moments can overload the 3 day old shotcrete and they can also permit deformations sufficient to allow failure propagation in the adjacent rock mass. This failure may have a detrimental influence on the loading of the lower legs of the arch when the bench is excavated.

In order to study the response of the support system to the excavation sequence and consequent tunnel deformations, a set of support capacity diagrams have been plotted in Figure 14. Note that the rockbolts are not part of the support system since they act as reinforcement and alter the properties of the rock mass surrounding the tunnel. Nevertheless these bolts play an important role in stabilizing the tunnel arch and in supporting the shotcrete shell.
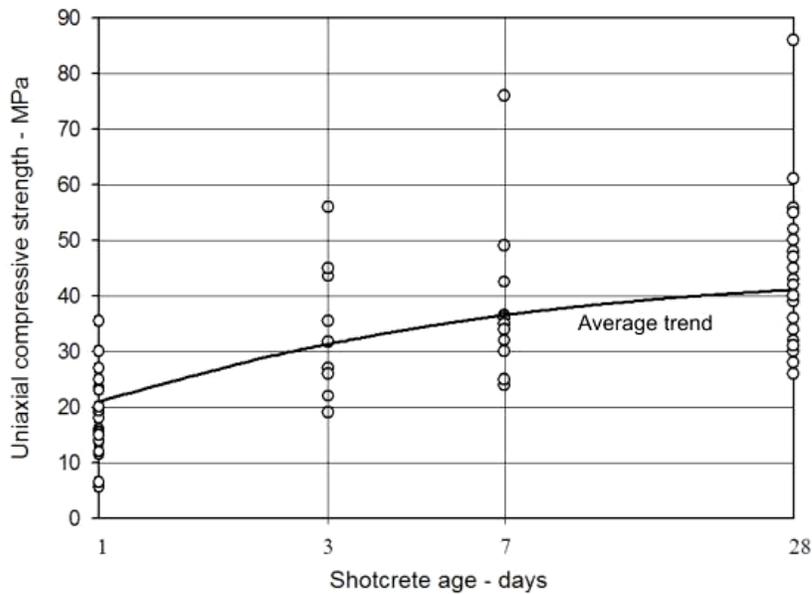
12

Figure 11. Uniaxial compressive strength development with time for shotcrete linings in tunnels around the world. After Melbye and Garshol (2000).

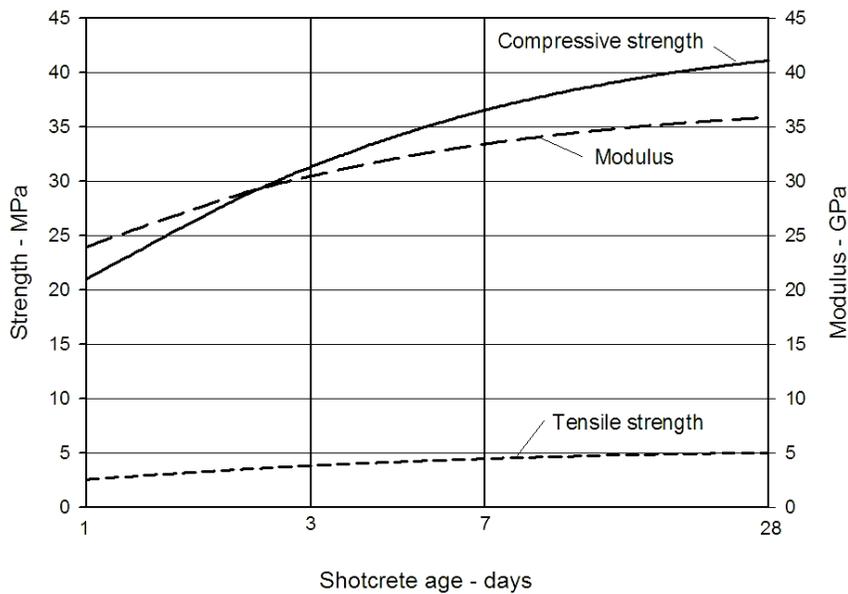

Figure 12. Assumed time dependent properties for shotcrete.

Table2. Excavation sequence and shotcrete properties

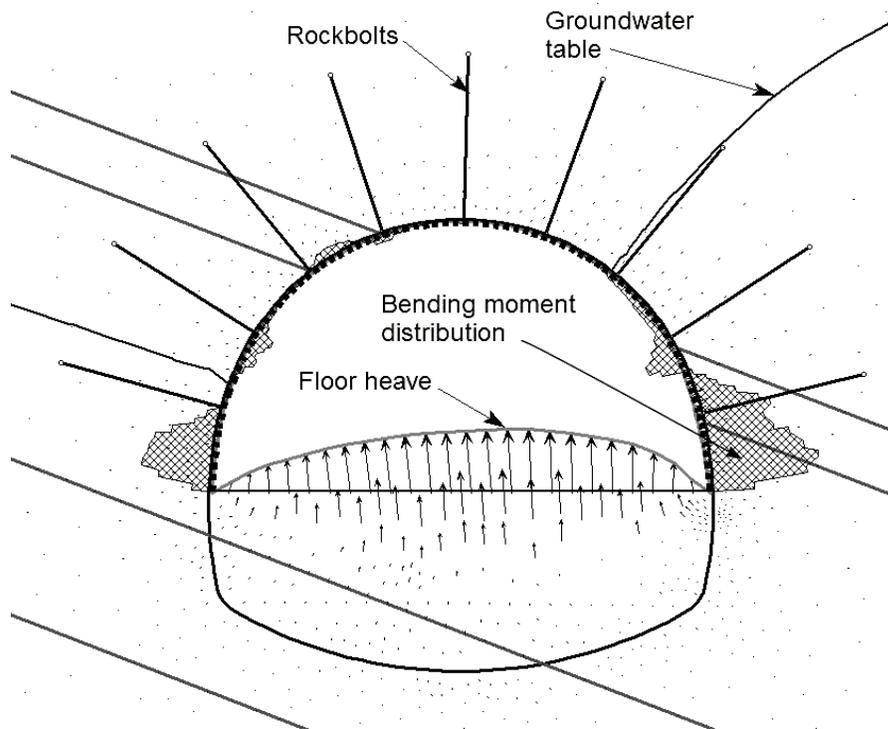|	Compressive strength σcsh	Tensile strength σtsh	Deformation modulus Esh
Day 1 – installation and activation of support	21.0 MPa	- 2.6 MPa	24,000 MPa
Day 3 –top heading convergence at about 10 m behind the face	31.0 MPa	- 4.0 MPa	30,000 MPa
Day 28+ - excavation of bench which may be as much as 1 year after top heading excavation	41.4 MPa	- 5.0 MPa	36,000 MPa

13

Figure 13. Bending moment distribution in the lining of the top heading with a flat unsupported floor on day 3 after installation of the support.

The derivation of the equations required to calculate these figures is given in Appendix 2. The calculation process results in a set of moment versus axial thrust and moment versus shear force diagrams for the lattice girders and the shotcrete. In the case of the shotcrete, the diagrams are calculated for 1 day, 3 day and 28 day strengths as defined in Table 2. From the numerical analysis, the axial forces, bending moments and shear forces in the installed top heading arch support are distributed onto the lattice girders and the shotcrete shell by means of equations A2.24 to A2.29 in Appendix 2. The resulting values, for the 1 day and 3 day loading conditions, are plotted as points in Figure 14.

Because of the shallow depth of the tunnel the axial loads carried by the support system are very low. Similarly, bending moments and shear forces in the lattice girders are small. However, the bending moments in the shotcrete lining are sufficient to exceed the capacity of the shotcrete at ages of 1 day and 3 days, as shown in the moment versus axial thrust diagram for the shotcrete, assuming a factor of safety of 1. This analysis illustrates that, for the in situ stresses, rock mass properties, excavation sequence and lining properties chosen, a top heading with a flat unreinforced and unsupported floor is not an appropriate choice.

The excessive bending moments in the lower portions of the top heading arch can be addressed in a number of ways including the installation of stressed anchors to limit the bending of the upper arch legs, increasing the thickness of the shotcrete shell, placing additional reinforcement in the lower arch legs or placing a temporary invert to limit the floor heave and the "pinching" of the arch. In this example, the placement of a temporary shotcrete invert will be investigated.

Examining Figure 14 may suggest to the reader that, since the loads carried by the lattice girders are so small, the shotcrete could be dispensed with and the lattice girders used on their own to carry the loads. This would be a serious mistake since these capacity plots are only valid when the lattice girders and the shotcrete act as a composite structure. The shotcrete, even when very young, provides lateral confinement for the lattice girders and this is essential to prevent buckling failure of these slender structures in the wide span tunnel.
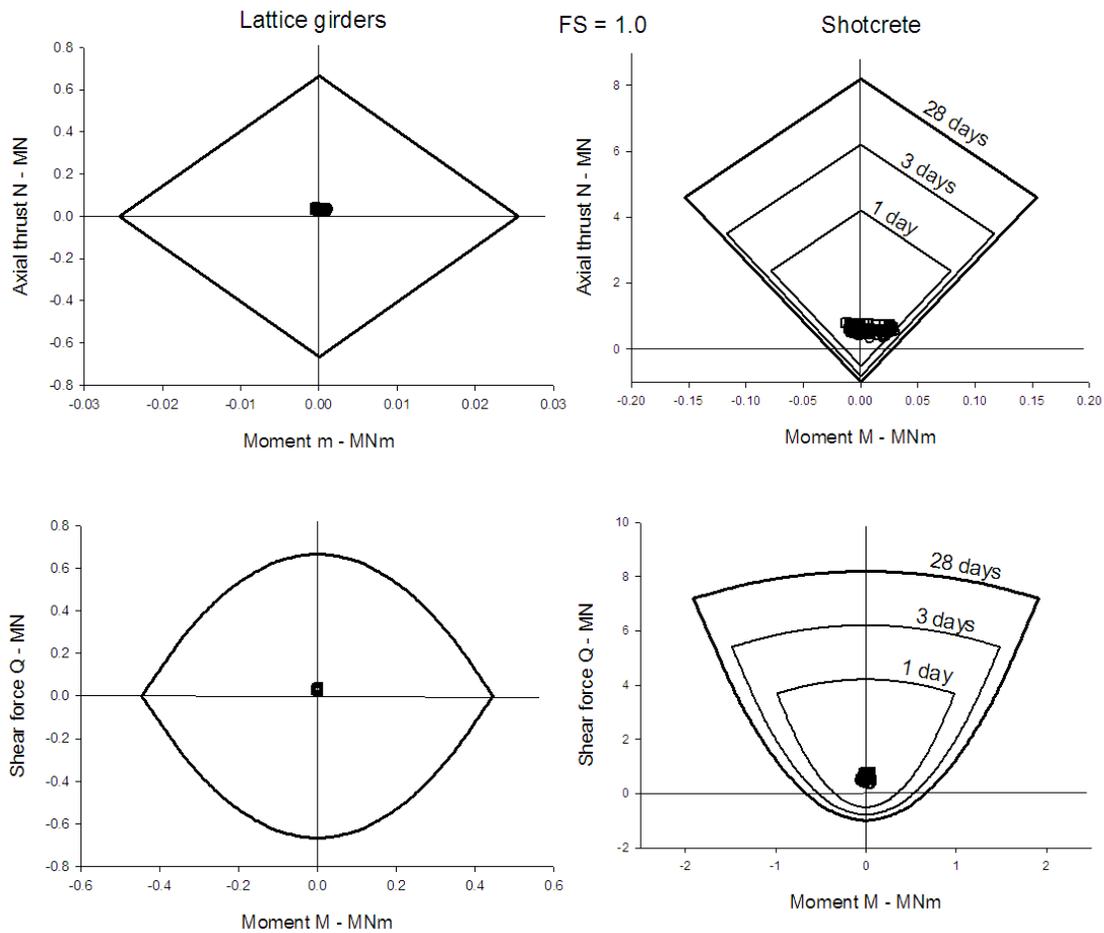
Figure 14. Support capacity diagrams for a 20 cm shotcrete lining, reinforced with 3 bar lattice girders, placed in a top heading excavation with a flat floor (see Figure 9).

2.8 *Analysis of top heading with a curved shotcrete invert*

A temporary shotcrete invert, such as that illustrated in Figure 15, is generally constructed from unreinforced shotcrete, typically 20 cm thick, so that it can be broken easily during benching. Backfill is placed over this invert in order to form a road surface for construction traffic.

It is important that a smooth connection is provided between this invert and the top heading arch legs in order to prevent the formation of stress concentration points. The shear capacity of the connection between the arch legs and the shotcrete invert can be deficient if the shotcrete is placed at different times. This problem can be overcome by adding reinforcement, such as that illustrated in Figure 16, to ensure that the loads in the arch are transferred into the invert. This reinforcement should be designed so that it can either be cut off or bent downward and incorporated into the lower arch legs when the temporary shotcrete invert is excavated.

A numerical analysis of top heading lining with a curved shotcrete invert covered by backfill results in the bending moment shown in Figure 17 and the corresponding support capacity plots given in Figure 18. In this case the analysis has been extended to include the removal of the bench and the placement and activation of the lower arch legs and the tunnel bottom invert. Since the structure of the arch legs is identical to the top heading arch it is permissible to plot the points for these two components on the same support capacity diagrams.

Figure 15. Top heading and bench excavation in a weak rock tunnel where a temporary shotcrete invert was used to control floor heave.
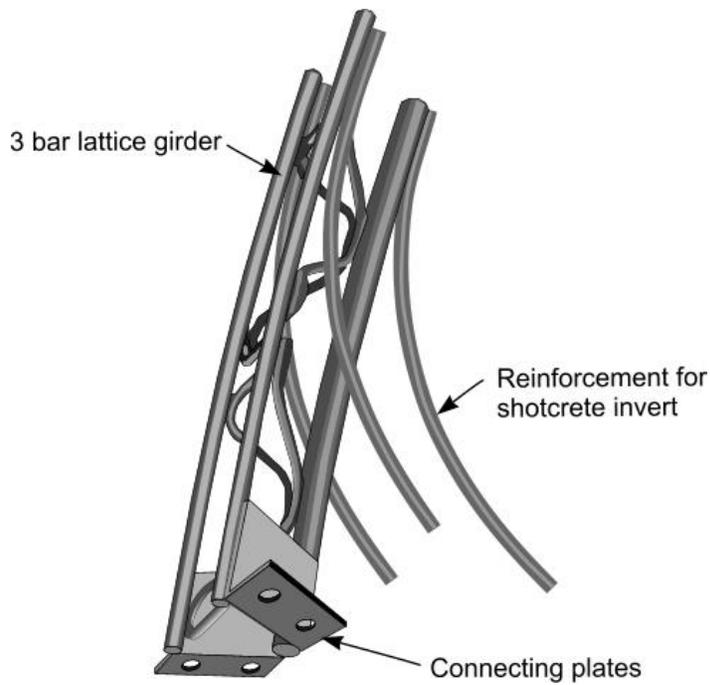

Figure 16. Additional reinforcement at the junction between the top heading arch legs and the temporary shotcrete invert.
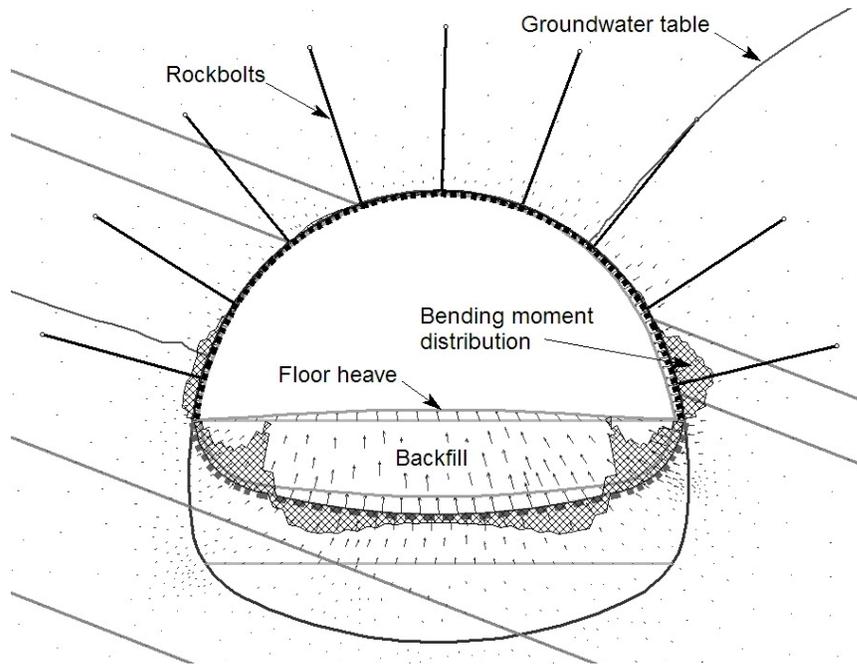
Figure 17. Bending moment distribution in a top heading lining with a curved shotcrete invert covered by backfill (see Figure 15).
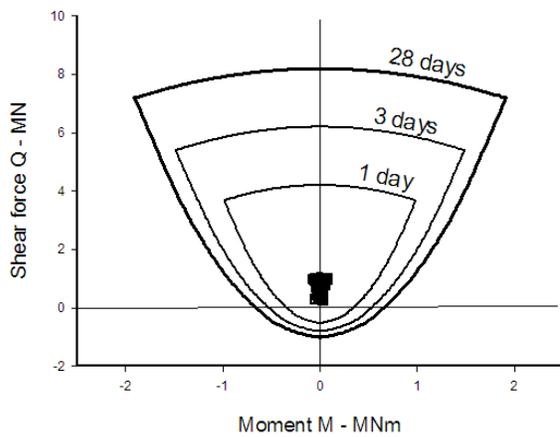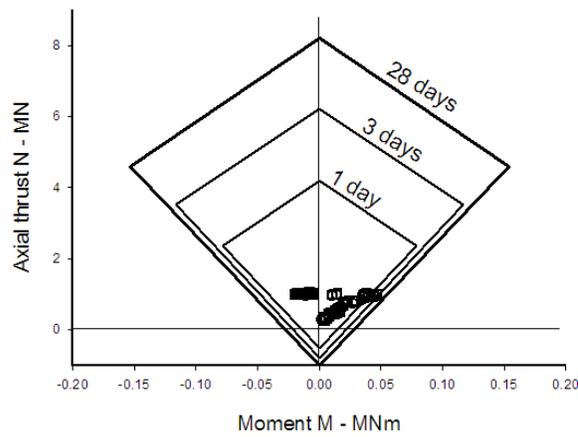

Figure 18. Support capacity plots for the 20 cm thick unreinforced shotcrete invert in Figure 17.

Figure 17 shows that the results of this analysis of the top heading arch are similar to those for the top heading with the flat floor, shown in Figure 13, except that the bending moments in the arch are reduced by the placement of the shotcrete invert. The support capacity plots for the un-reinforced invert, given in Figure 18, show that the bending moments induced in the invert are just sufficient to induce tensile cracking in the 1 day and 3 day old shotcrete. While this would be a problem elsewhere it is considered to be acceptable here since the shotcrete invert is constrained by the overlying backfill and some minor cracking will be of little consequence. However, if the designer is uneasy about this cracking or if the client is reluctant to accept any indication of failure, the invert can be made thicker or it can be reinforced with polypropylene fibers to increase its capacity.

The support capacity plots for the shotcrete arch and lower legs for the case of the curved shotcrete invert are shown in Figure 19. The Moment-Axial thrust points for the shotcrete all fall well within the capacity curves for the corresponding age of shotcrete. This confirms that the use of the shotcrete invert has reduced the bending moments that resulted in problems in the top heading excavated with a flat floor (Figure 14).

A check on the invert on the bottom of the tunnel shows no overstressing and, hence, the complete lining is stable and the design can proceed to the installation of the final lining. Note that, if there is a large time delay (say for more than 1 year) between the excavation of the tunnel and the installation of the final lining, it may be necessary to recalculate the lining forces for a reduced rock mass strength to allow for time-dependent deterioration.
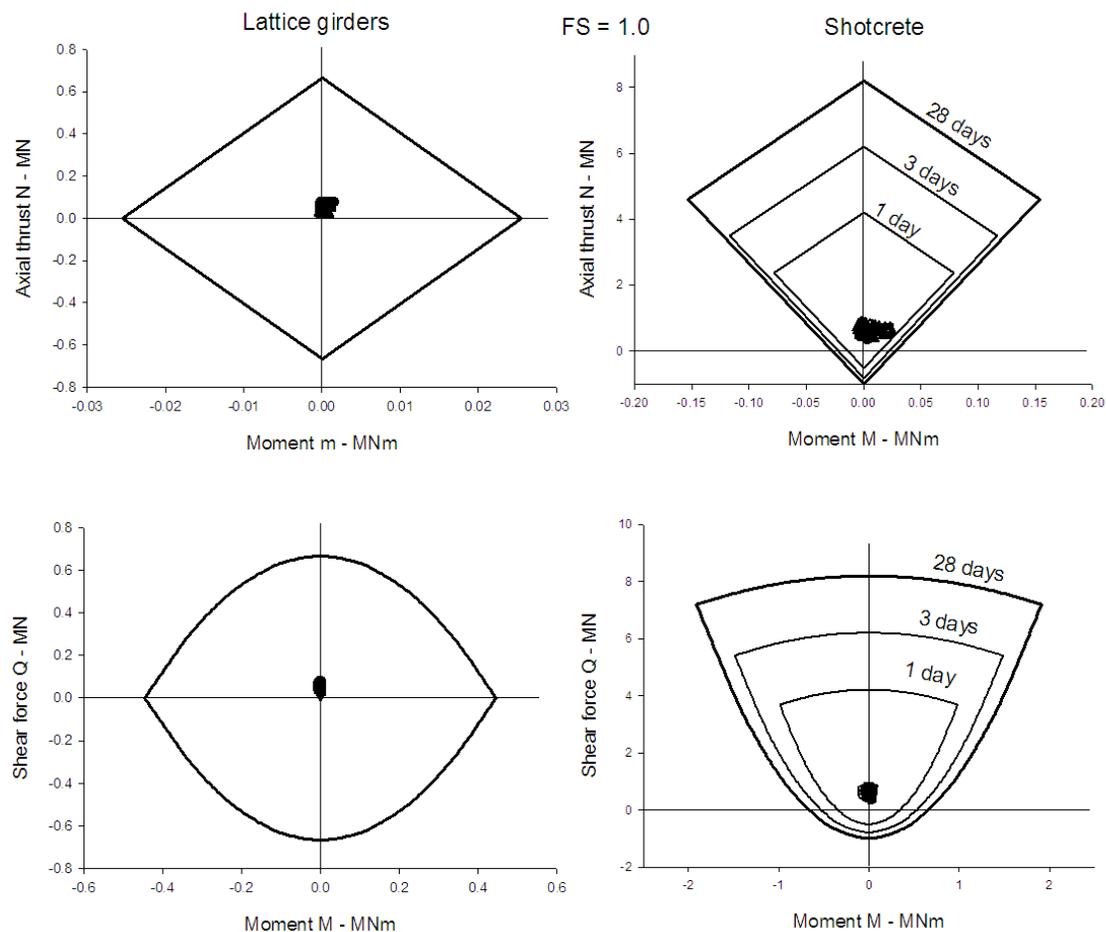

Figure 19. Support capacity diagrams for a 20 cm shotcrete lining, reinforced with 3 bar lattice girders, placed in a top heading excavation with a curved shotcrete invert (see Figure 15).

The next step after the excavation and stabilization of the full tunnel profile is the installation of a final lining. The typical geometry of this lining was shown in Figure 4 and it is given in detail in Figure 20. In this example it is assumed that the final lining itself consists of 30 cm thick cast-in-place concrete reinforced by means of 20 mm diameter steel reinforcing rods spaced at 18 cm x 22 cm apart.

For simplicity the properties of the cast in place concrete final lining are assumed to be the same as those of the initial shotcrete lining, as defined in Table 2. Because the final lining is installed in a stable tunnel it carries no initial load except for its self-weight. Hence, only the 28 day properties are relevant in the following calculations. Loads are imposed on the final lining as a result of stress changes, changes in the groundwater conditions, changes in the characteristics of the initial support system or deterioration of the rock mass surrounding the tunnel. All of these changes are assumed to occur in this example and the consequences will be examined in the analysis that follows.
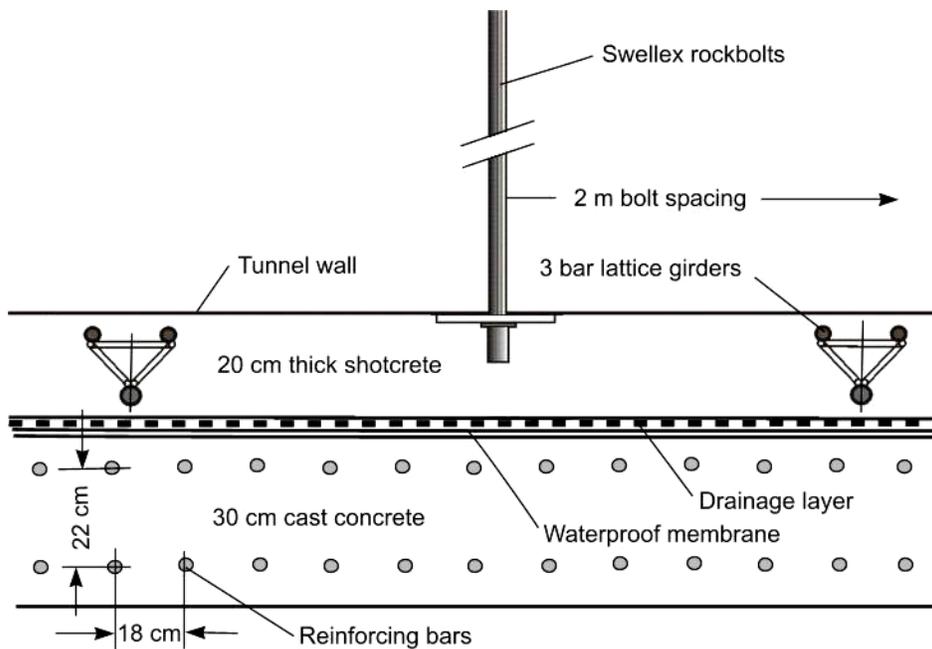

Figure 20. Geometry of composite final lining consisting of a 20 cm thick initial shotcrete lining, a drainage layer, a waterproof membrane and a 30 cm thick cast concrete lining (Not to scale).

After the installation of the final lining the open cut for the adjacent highway carriageway is excavated as defined in Figure 1. This results not only in changes in the stress field surrounding the tunnel but also changes in the groundwater conditions as defined by curve C in Figure 3. In designing the final lining these changes have to be accommodated and a factor of safety in excess of 2.0 has to be provided by the lining for these "normal" loading conditions.

The long term loading conditions, for which a factor of safety of 1.5 has been specified for this example, include corrosion of all the rockbolts, blockage of the tunnel drains and deterioration of the rock mass surrounding the tunnel. Other extraordinary long term-loading conditions may apply in specific cases and these should also be included. Basically, the aim of the designer should be to ensure that the tunnel will remain stable and operational under all possible conditions that could occur during its service life.

The participation of the initial shotcrete lining has been a matter of contention for many years. Until relatively recently tunnel designers in some countries were required to ignore the contribu-

tion of all initial reinforcement and shotcrete linings in calculating the support capacity of the final lining. However, this very conservative approach has changed and the International Tunnelling Association's Guidelines for the Design of Tunnels (1988) gives the following recommendation: "An initial lining of shotcrete may be considered to participate in providing stability to the tunnel only when the long-term durability of the shotcrete is preserved. Requirements for achieving long-term durability include the absence of aggressive water, the limitation of concrete additives for accelerating the setting (liquid accelerators), and avoiding shotcrete shadows behind steel reinforcement".
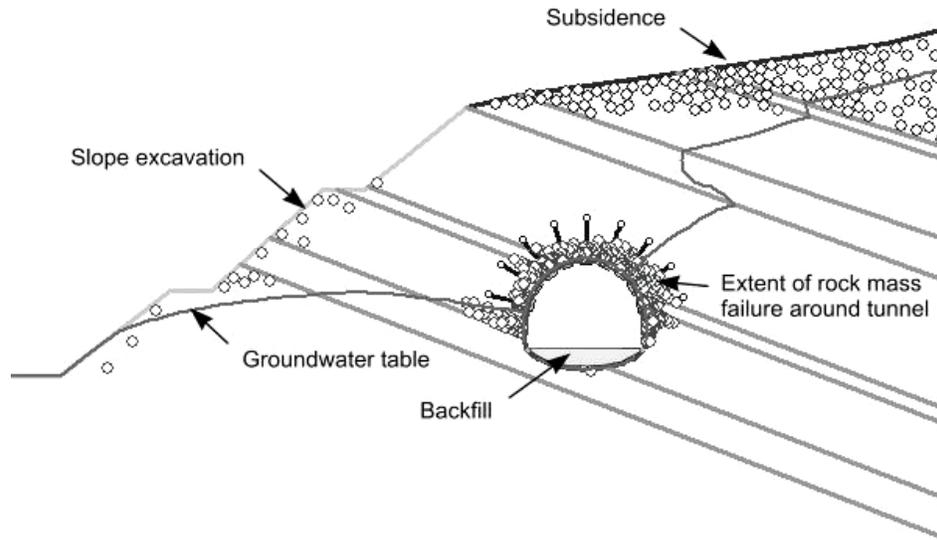

Figure 21. Changes in stress and groundwater conditions as a result of excavation of the open cut for an adjacent carriageway can result in propagation of failure zones in the rock mass.
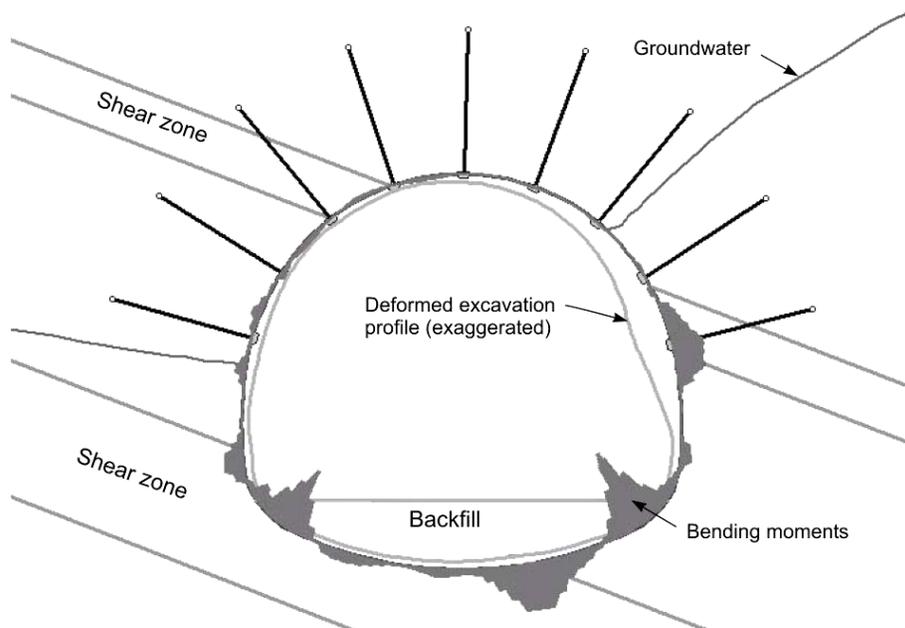

Figure 22. Distribution of bending moments and deformations of the final tunnel profile after installation of the final lining and excavation of the adjacent cut.

The extent of rock mass failure surrounding the tunnel, after installation of the final lining and excavation of the adjacent open cut is shown in Figure 21. Note that some rock mass failure of the surface occurs as a result of surface subsidence and stress relief due to the open cut excavation. While this is not significant in the design of the tunnel lining it does highlight the need for the designer to check on surface subsidence and slope stability issues. In shallow tunnel such as this one, caving to surface can be a critical issue and it has to be checked very carefully during the sequential excavation of the tunnel.

The bending moments and the deformations induced in the final lining are shown in Figure 22. Note that the presence of the two shear zones has a significant influence of these distributions, particularly on the right hand side of the tunnel arch. As shown in the support capacity plots in Figure 23, these bending moments are the most significant forces to be considered in the lining design since all other forces are very low.

Detailed plots of the moment-thrust relationships for the final lining for three model stages are given in Figure 24. These show that the lining carries practically no load at the time of installation. The forces in the lining change slightly when the adjacent open cut is excavated and they change by a significant amount when the long term loads are applied. These loads are induced by a reduction of the residual strength of the failed rock surrounding the tunnel, an elimination of all rockbolts and changes in the groundwater conditions as a result of blockage of the drains. The factor of safety for the lining for these long term loads is approximately 2.0.
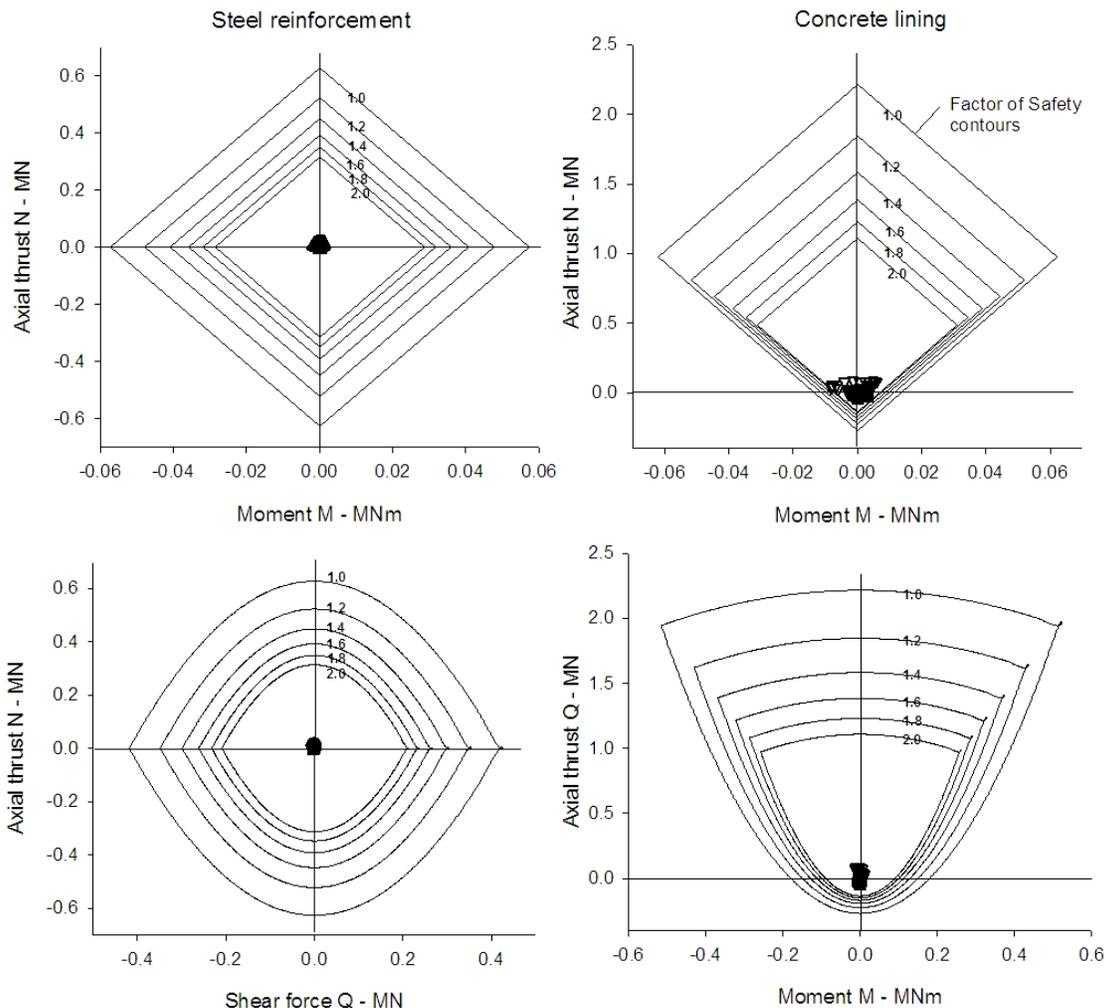

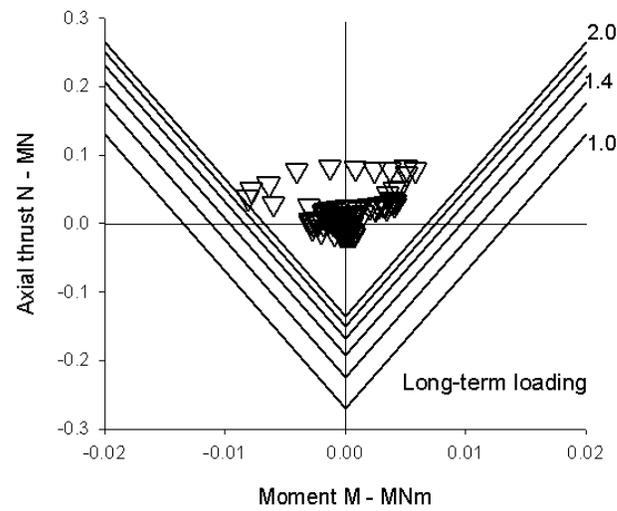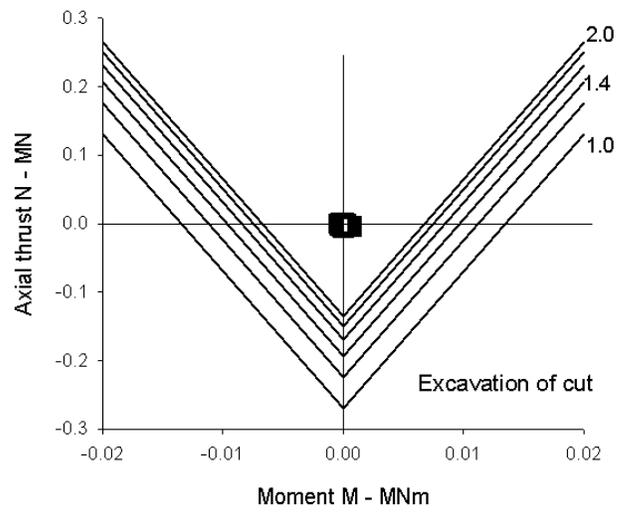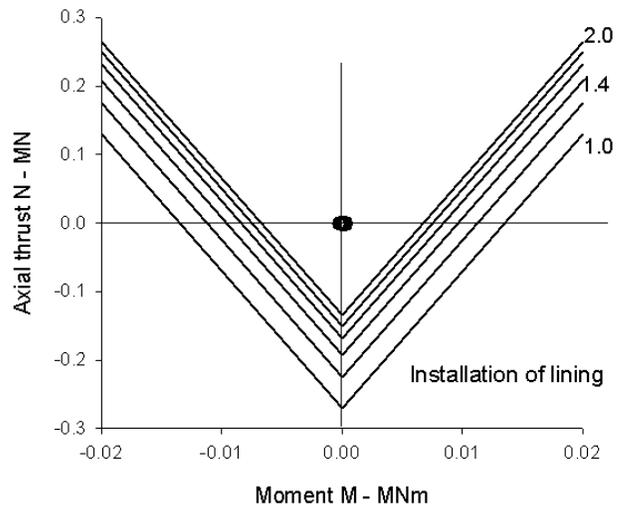Figure 23. Support capacity plots for the final concrete lining.

Figure 24. Detail of moment versus axial thrust development in the final concrete lining from the installation of the lining, the excavation of the open cut and long-term loading conditions.
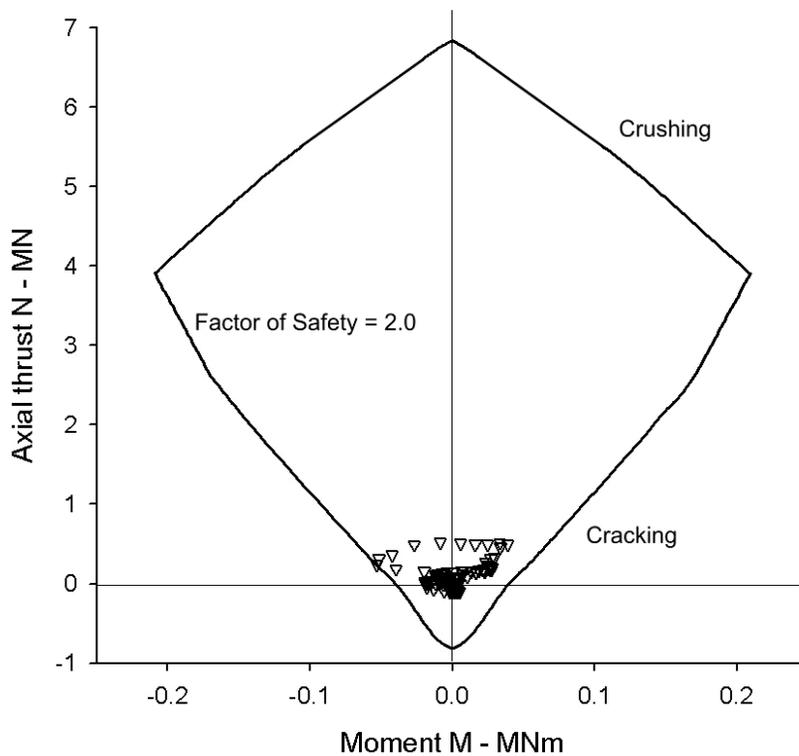
Figure 25. Minimum Moment-Thrust capacity for the reinforced concrete final lining calculated by the structural program Response 2000 (Bentz, 2000) for a factor of safety of 2.0.

Figure 25 gives a minimum moment-thrust capacity diagram for the reinforced final lining for a factor of safety of 2.0, generated using the structural program Response 2000 (Bentz, 2000). This is a sectional analysis program that will calculate the strength and ductility of a reinforced concrete cross-section subjected to shear, moment, and axial load. All three loads are considered simultaneously to find the full load-deformation response using the modified compression field theory (Vecchio and Collins, 1986).

The total moment-thrust points for the final lining under long-term loading conditions are also plotted in Figure 25. The relationship of these points to the capacity curve, defined by cracking of the concrete, is similar to that illustrated in Figure 24 for the concrete component of the lining. This comparison serves as a confirmation that, at least for the low load considered in this example, the elastic support capacity plots derived in Appendix 2 are an appropriate tool to use for reinforced concrete lining design.

The separation of the forces in the concrete (or shotcrete) and the steel reinforcement, as has been done in Figures 19 and 23, gives information on the contribution made by each of these components and on the combination of forces that control the design process. In this example the bending moments in the concrete are by far the most important forces and, when combined with the relative low tensile strength of concrete, they determine the performance of the lining.

3 CASE HISTORY 2 – A DEEP TUNNEL IN WEAK GROUND

This case history is based on the Yacambú-Quibor tunnel currently under construction in the Northern Andes in Venezuela. Aspects of this project are described by Guevara (2004). Design and construction details are simplified for the purposes of this example. This analysis involves new construction within the central portion of a 25 km tunnel, 5.2 m in diameter, in highly variable metamorphic rock at depths of up to 1200 m below surface (Figure 26).

a) longitudinal topographic profile (north to the right)

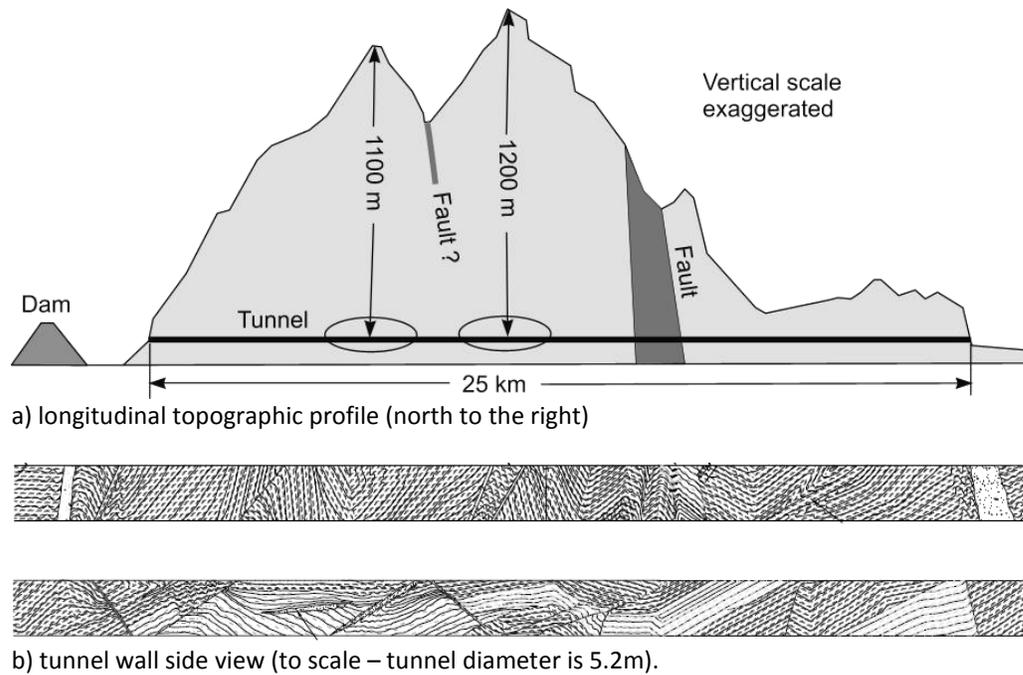b) tunnel wall side view (to scale – tunnel diameter is 5.2m).

Figure 26. a) Longitudinal topographical profile along tunnel alignment. Major regional faults are shown. Ellipses indicate zones of interest for this case study. b) Two typical tunnel wall maps showing high variability in geological structure and fabric alignment.

The tunnel is designed for water transport, under moderate velocity and head, from a rainforest region in the south to an agricultural centre to the north. The tunnel will include the facilities to drain and inspect the tunnel with vehicle access after construction and during service life.

The design problem discussed here relates to a typical tunnel profile in highly deformed graphitic phyllite (Figure 27). The deformation in the rock mass is the result of the tectonic processes inherent in the Andes Mountains and is also the result of the proximity of the tunnel to a large regional fault related to the intersection of three major crustal plates. The fault passes through the tunnel as seen in Figure 26. A second fault has been identified on surface but it is not known whether this will be intersected at tunnel depth. This analysis is related to the section of tunnel identified in this figure where the average depth of overburden is approximately 1150 m. The in situ stresses at depth are assumed to be approximately equal (30 MPa) in all directions as a result of the low shear resistance due to the fact that the tectonic history of the rock mass has reduced its properties to their residual values.

Tests on intact core samples of this rock gave uniaxial compressive strength values of 15 MPa to 110 MPa (Salcedo, 1983). The high variability in results is due to the orientation of the phyllitic foliation with respect to the loading direction. As seen in Figure 27, the rock mass in the tunnel is tightly folded and no particular orientation of fabric presents itself over a significant portion of the tunnel profile. On the scale of the tunnel, therefore, isotropic rock mass strength can be assumed. Back analyses of monitored sections of the excavated tunnel confirm that the average uniaxial compressive strength of the intact graphitic phyllite is approximately 50 MPa and this value has been assumed for this analysis.

The rock mass was assessed using the Geological Strength Index (GSI) system (Marinos and Hoek, 2001) and rock mass strength parameters, according to Hoek et al. (2002), are shown in Figure 28. A GSI value of 25 is assigned to the rock mass over this section of the tunnel. As the rock mass is already in a deformed (residual) state, it is assumed to act plastically in response to stress change and deformation. The long term strength of the rock mass is assumed to correspond to moderate disturbance according to the GSI system with a Disturbance factor D = 0.2. The deformation modulus of the rock mass is estimated to be 1650 MPa, based on the methodology of Hoek and Diederichs (2006).
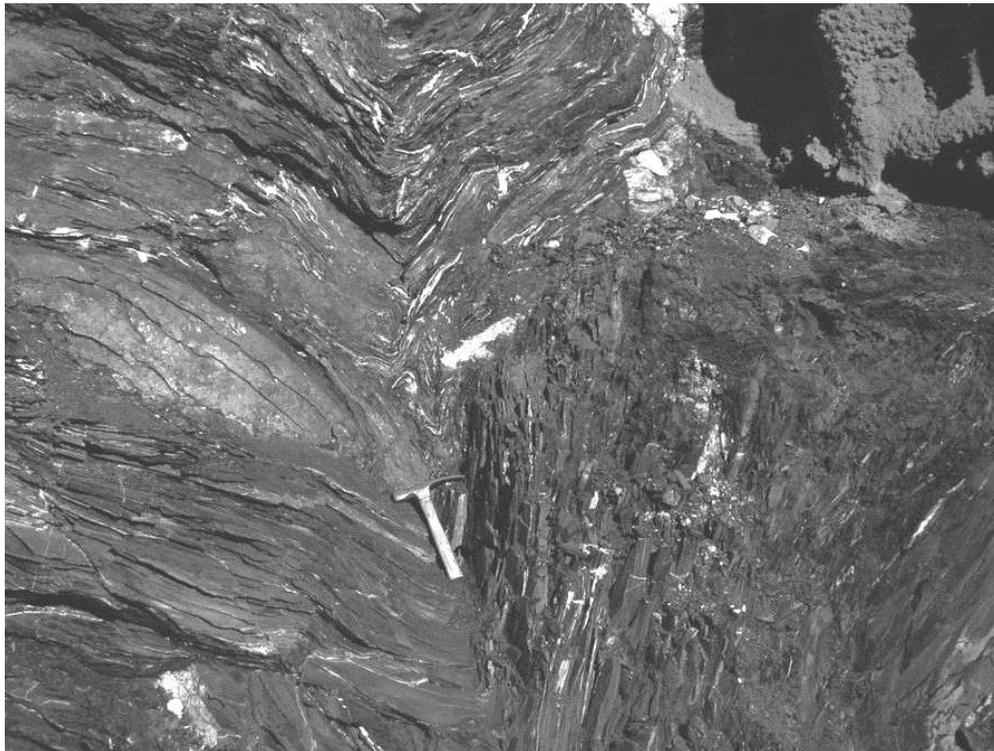
24

Figure 27. Graphitic phyllite in the tunnel face. Note the tight secondary folding and high variability of fabric orientation – rock hammer in center is 45cm long.
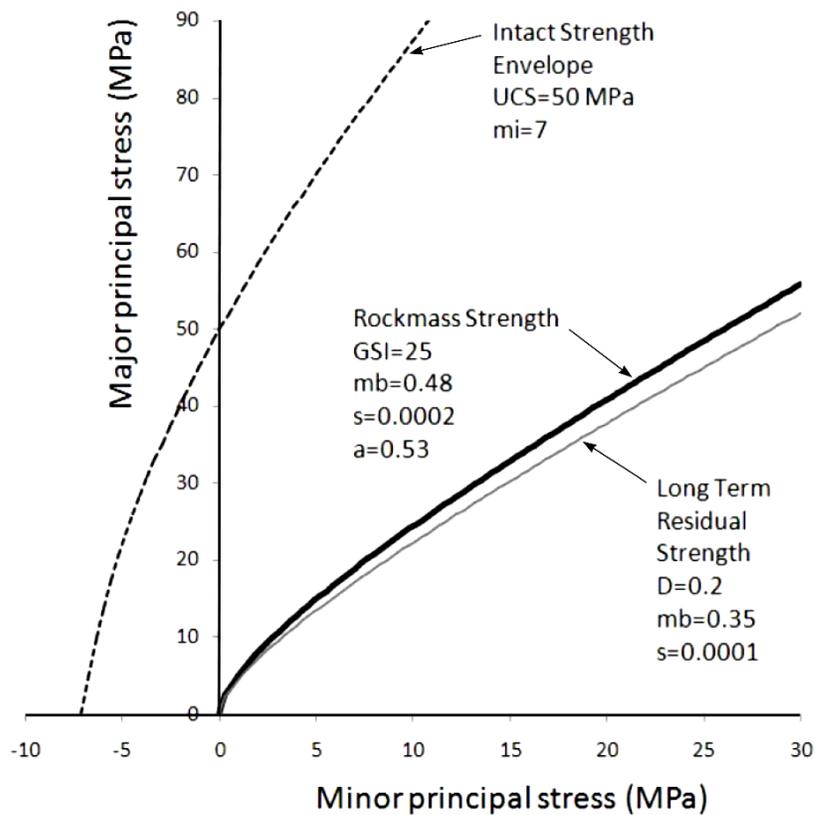

Figure 28: Rock mass strength parameters for Case 2 analysis. In situ stress = 28MPa.

Tunnelling in these conditions is extremely difficult (Hoek and Marinos, 2000). Preliminary analysis of an unsupported tunnel in this rock mass at this depth indicates closure in excess of 50%. The key to liner design is to sequence the installation of support to avoid overload while still maintaining a safe working environment at and near the face.

Numerous challenges have been encountered over the long history of this construction project (a complete history of which is beyond the scope of this paper) and, due to the high cost of an additional concrete lining, it has been decided that the support system installed during construction will act as the final lining. In addition to resisting cracking and spalling this liner must control displacements to preserve the minimum tunnel size required for vehicular access during operation.

After several iterations in liner design over the years, each with its own lessons, the current design was adopted. A circular profile with steel arches (W6 X 20) at 1 m intervals, embedded in 60 cm of shotcrete applied in two passes of 20 cm and 40 cm thickness, is specified. There is a requirement to install support early to provide a safe working space at the face. Activation of the full lining, however, has to be delayed to prevent an unacceptable build-up of internal loads due to the high closure rates near the tunnel face. Premature installation of the final lining could result in buckling of the primary support system, associated expansion of the plastic zone and increase in final closure.

Specifications for the support were based, in part, on analytical convergence-confinement calculations (Carranza-Torres and Fairhurst, 2000). In this analysis, illustrated in Figure 29, the liner is treated as a single 60 cm thick concrete shell enclosing one W6 x 20 steel set per metre. The relationship between wall displacement and location along the tunnel (the linear displacement profile) is estimated based on the methodology described in Appendix 1 for a normalized plastic zone radius *Pr* of 6.5. Installation of the full liner near the face results in a low short term factor of safety and an unacceptable long term factor of safety of approximately 1.0. This long-term factor of safety is increased to approximately 1.4 with the installation of sliding joints. This prediction for the supported tunnel is conservative as it ignores the overall displacement reduction due to rock-support interaction.
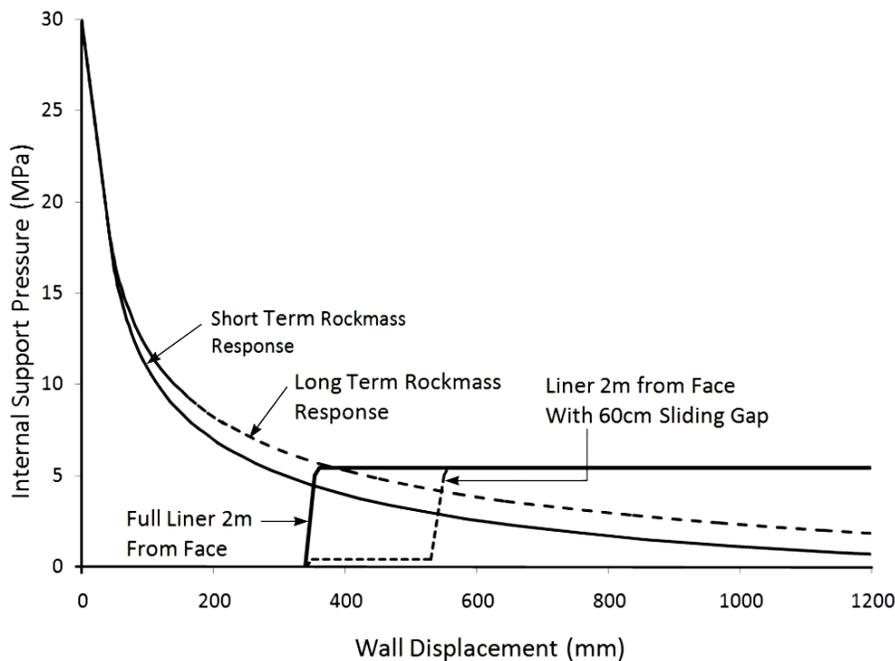

Figure 29. Convergence confinement analysis (according to method of Carranza-Torres and Fairhurst, 2000) for short and long term ground response (unsupported). Liner load development for 60 cm shotcrete section with W6 x 20 steel section. Dashed support load curve represents delayed loading due to sliding joint.

26

Sliding joints, shown in Figure 30, allow controlled convergence (closure) of the steel sets without excessive loading of the steel. These joints provide resistance against moments but allow slip at low axial loads until the gap is closed. At this time the liner builds up load as a closed circle. The sliding joint is fabricated on site using two heavy steel plates constraining the set flanges through the tensioning of bolts as shown in the inset in Figure 30. The opposing steel sections are clamped by this device with a controlled gap (in this case 25 to 30 cm). This technique has proved to be very effective at Yacambú-Quibor. Alternative yielding support systems have also been widely used in squeezing ground conditions in Europe (Schubert, 1996).

Figure 30. Circular steel arches (W6 X 20) with two sliding joints (detail in inset).

The original design called for the complete steel set to be erected near the face and a 20 cm layer of shotcrete sprayed over the sets with 1 m gaps left over the sliding joints as shown in Figure 31. The two sliding joints are installed just below the spring line for a total circumferential closure of 60 cm (2 x 30 cm). Once the gap is closed by tunnel deformation, the gap is filled with shotcrete and an additional 40 cm of shotcrete, reinforced by means of circumferential rebar, is applied to the inside of the liner. The effect of the sliding gap is illustrated by the dashed support response line in Figure 29. This simple convergence-confinement analysis does not consider moments and neglects the interaction between support layers. In addition the stabilizing effect of the liner and the resultant reduction in rock mass displacement are not considered. Nevertheless, this analysis correctly indicates the need for delayed loading of the liner.

   Due do difficulties with face instability, the contractor found it necessary to implement the support system in two stages with a short 1.5 m bench (from floor to springline) maintained to buttress the face. The upper semicircular section of the steel set is installed at the face to provide a primary safety system. The arch sections rest on the bench and are covered in shotcrete. The bench is then excavated approximately 1.5 m from the face and the circular arch, including the pair of sliding joints, is completed. The first 20 cm shotcrete layer is completed at this stage (Figure 32a).

   A reinforcement cage is assembled adjacent to the initial shotcrete lining as seen in Figure 31. Once joint closure is achieved (within 5 to 15m of the face) the gap is closed with shotcrete to complete the final 40 cm thick final lining. The final lining section is illustrated in Figure 32b.

Figure 31. Initial Liner composed of circular steel arch and 20 cm of shotcrete. Inset shows detail of sliding joint with shotcrete gap. Note rebar in place to reinforce final shotcrete layer.
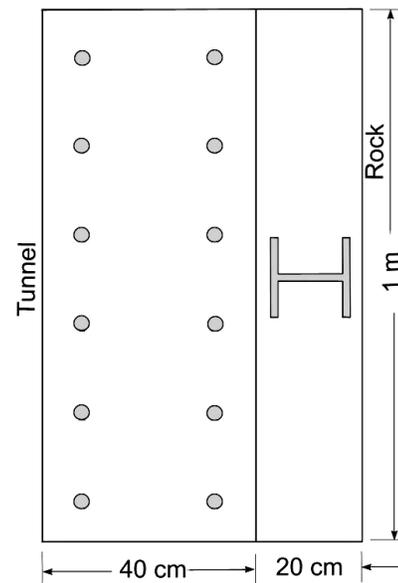
a)   b)

Figure 32. a) Configuration of mid-height bench (partially disintegrated in this photograph) and upper steel arch installed ahead of lower section and sliding joint. b) Final 60 cm section with outer shotcrete and steel set composite section and inner reinforced shotcrete section. The tunnel is to the left and rock mass is to the right of the section.

The following analysis represents a more rigorous consideration of the interactions between the liner components and the construction sequence. The first step in the design process is to determine the normalized maximum unsupported failure radius via a simple plane strain analysis of the unsupported tunnel. In this case, the ratio of maximum plastic radius to tunnel radius is 6.5.

Next, the longitudinal deformation profile can be calculated using the methodology given in Appendix 1. Alternatively, since the stresses are isotropic and the tunnel is circular, an axisymmetric model (Figure 33b) can be used for this purpose. A longitudinal deformation profile for the unsupported tunnel is shown as a dashed line ("Disp. vs Distance") in Figure 33a. An estimate of the displacement profile for the supported tunnel (with liner and sliding joints) is presented in Figure 33a as a dotted line for comparison.

A 2D finite element plane strain analysis is then applied to the full face construction sequence (unsupported). The technique of progressive face replacement described in the previous section (Figure 7) is used here. The resulting points on the ground reaction curve (white diamonds on "Disp. vs Support Pressure" curve in Figure 33a) can be assigned locations along the tunnel (filled diamonds in Figure 33a) using the (dashed) longitudinal deformation profile.
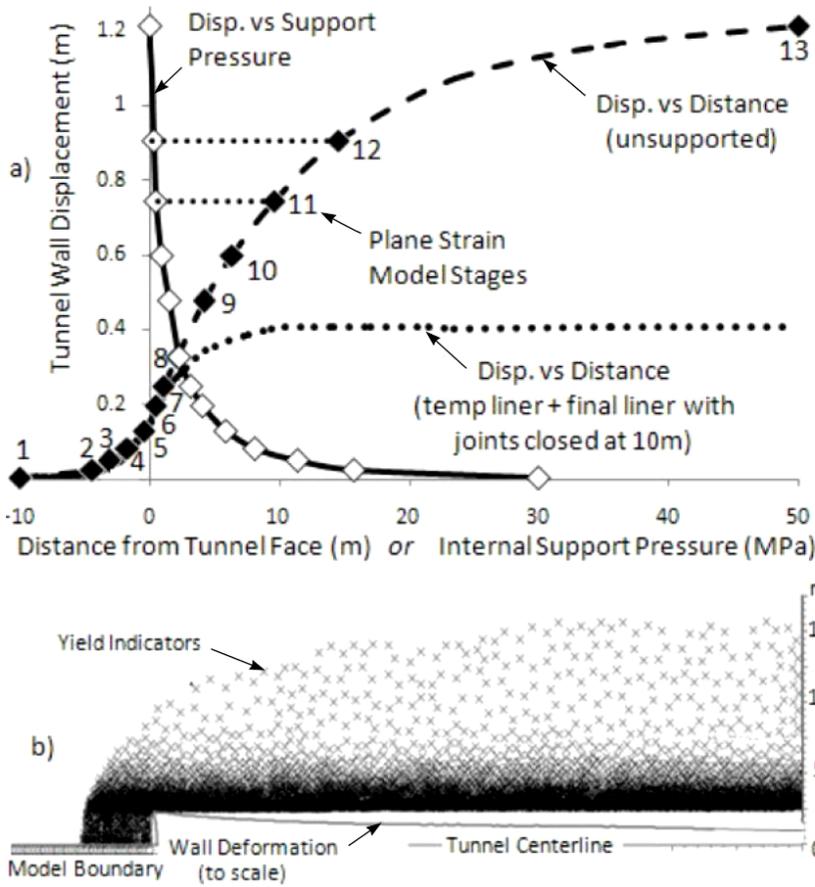
Figure 33 a) Ground reaction curve "Disp. vs Support Pressure" and corresponding longitudinal displacement profile "Disp vs Distance (unsupported)" for a axisymmetric model. Normalized plastic radius = 6.5. Longitudinal displacement profile function fitted based on Appendix 1. Point symbols and number ID's represent corresponding stages in plane strain model (related symbols are linked between two curves as shown for stage 11 and 12 by dotted lines). Supported longitudinal deformation profile (dashed line without symbols) shown for comparison. b) Axisymmetric model used for calibration showing yield indicators (x's) and wall displacement along tunnel (Vlachopoulos & Diederichs 2009b).

29

Figure 34. Finite element mesh, geometry of excavation stages and liner segments for 2D plane strain analysis of sequenced excavation and support.

The same correlation of model stage to tunnel location can be used for the benched tunnel model with offset stages of bench excava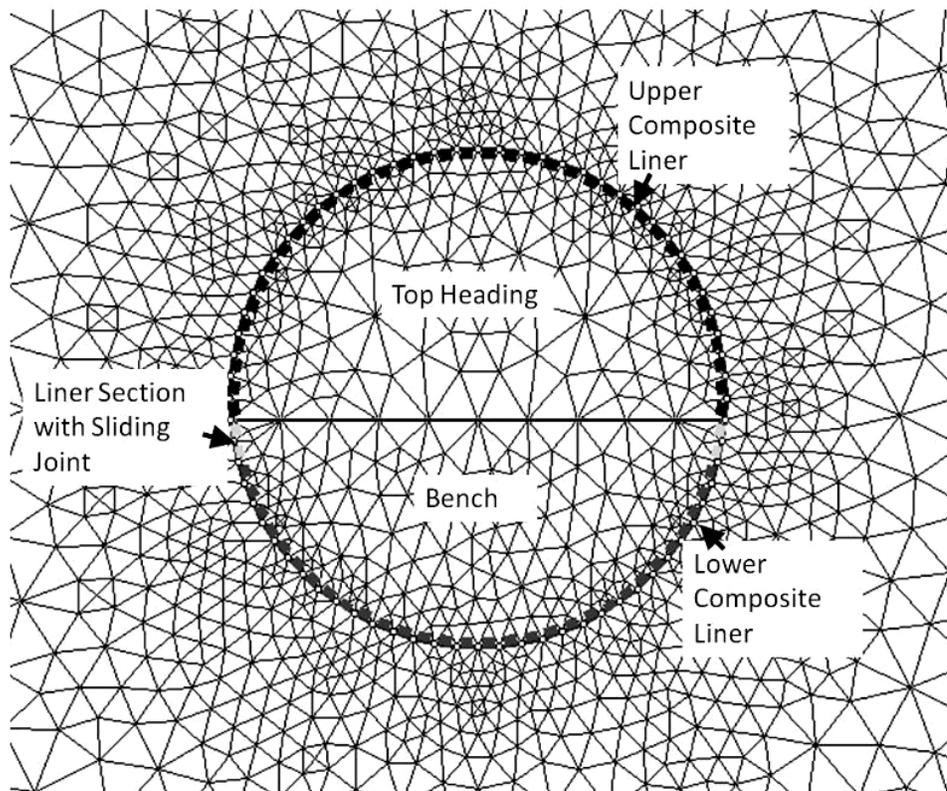tion and with appropriate installation of support (remember that the model support is installed at the beginning of the stage while the displacements are reported at the end of the stage). The benched tunnel model is illustrated in Figure 34.

It is anticipated that the steel sets and the initial 20 cm shotcrete layer will undergo some limited yielding after the sliding joints close. The upper half of the arch, installed in the bench, may also yield prior to this due to the moments induced by a reduction in the arch radius. This partial arch and the complete arch, with sliding joints, are modeled as separate but joined layers with appropriate material and section properties. They are assumed to act plastically with yield in the steel and a 33% reduction in residual uniaxial compressive strength of the shotcrete after yield.

Following the geometry in Figure 34, the bench excavation sequence lags behind the top heading by 2 stages. The upper composite liner is installed immediately behind the face (start of stage 7 in Figure 33). The lower composite liner and the sliding joints are installed approximately 1 m behind the bench (beginning of stage 9), and the filler sections of 20 cm shotcrete are installed and assumed to set by the beginning of stage 10. In this analysis the sliding joint gap closes automatically two stages later (within stage 11) between 6 and 10 m form the face.

The final lining is applied behind the gap closure, beginning of stage 12 (10 m from the face) for this analysis. This final lining is applied as an elastic composite according to the methodology in Appendix 2. For the purposes of this analysis, a symmetrical reinforcement array of 6 x 25 mm rebar per metre, 75 mm from each surface is used. The moment of inertia, section depth and total area are calculated for the rebar arrangement. The procedure is then similar as that described in Appendix 2 for steel sets. The relevant properties are given in Table 3.

The aging of shotcrete is neglected here as the excavation rate is very slow (approximately 1 m per day). The shotcrete used at the site was of very high quality and 7 day strength and stiffness values are used.

30

The short- and long-term liner loads are shown in Figure 35 for the full face excavation and for the top heading and bench option. The compromise required to provide a bench for face support results in a less uniform loading of the two halves of the arch and the build-up of moments in the sliding joint area. This effect is exaggerated dramatically if the final lining is installed before the sliding gap has closed.
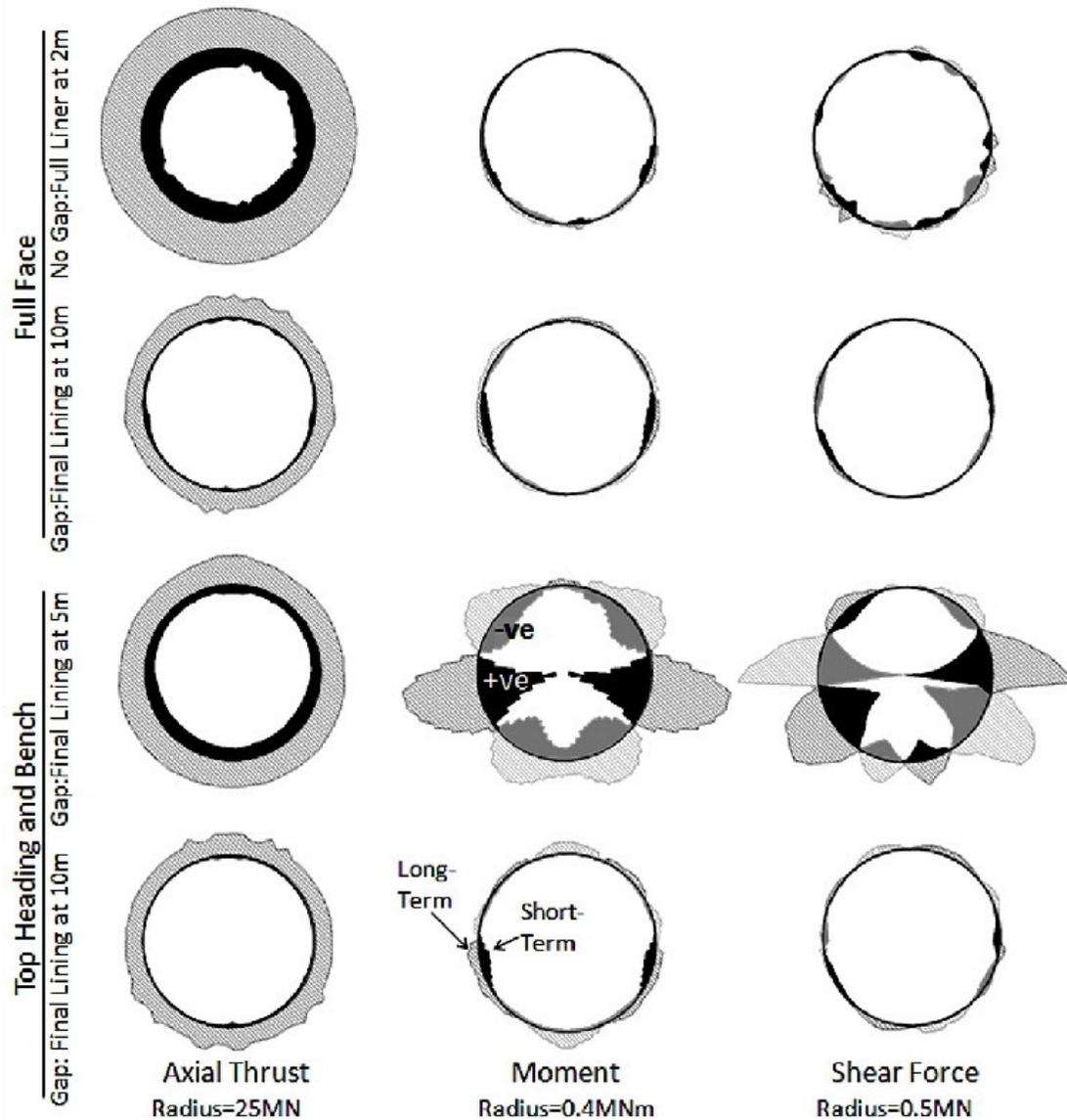
Figure 35. Relative magnitudes and distribution of total axial load, moment and shear load in the final 40 cm thick reinforced layer. Values plotted inside tunnel as solid represent short term loading conditions. Hatched values outside of tunnel represent long term conditions. Dark shading indicates positive values for moment and shear, light shading indicates negative values. This inner final liner layer is modeled elastically. This plot does not include residual loadings in the plastic outer lining layer (steel sets embedded in 20 cm shotcrete).

To analyze the loadings within the steel and concrete components of the final inside lining layer, the equations in Appendix 2 are used to partition the loads and moments and to generate elastic capacity envelopes for comparison as shown for the full face options in Figure 36.

Table 3. Liner properties for reinforced 40 cm inner liner (for use with Appendix 2).

Tunnel Radius		2.52	m	Width of Section		1	m
Rebar Properties				Shotcrete Properties			
Number of Pairs per Section		6		Height of Section		0.4	m
Height of Rebar Section		0.25	m	Young's Modulus		30000	MPa
Area of Section		0.005985	m^2	Poisson's Ratio		0.2	
Moment of Inertia		9.40E-05	m^4	Compressive Strength		40	MPa
Young's Modulus		200000	MPa	Tensile Strength		-4	MPa
Poisson's Ratio		0.3					
Compressive Strength		400	MPa				
Tensile Strength		-400	MPa	Number of sets n		1	
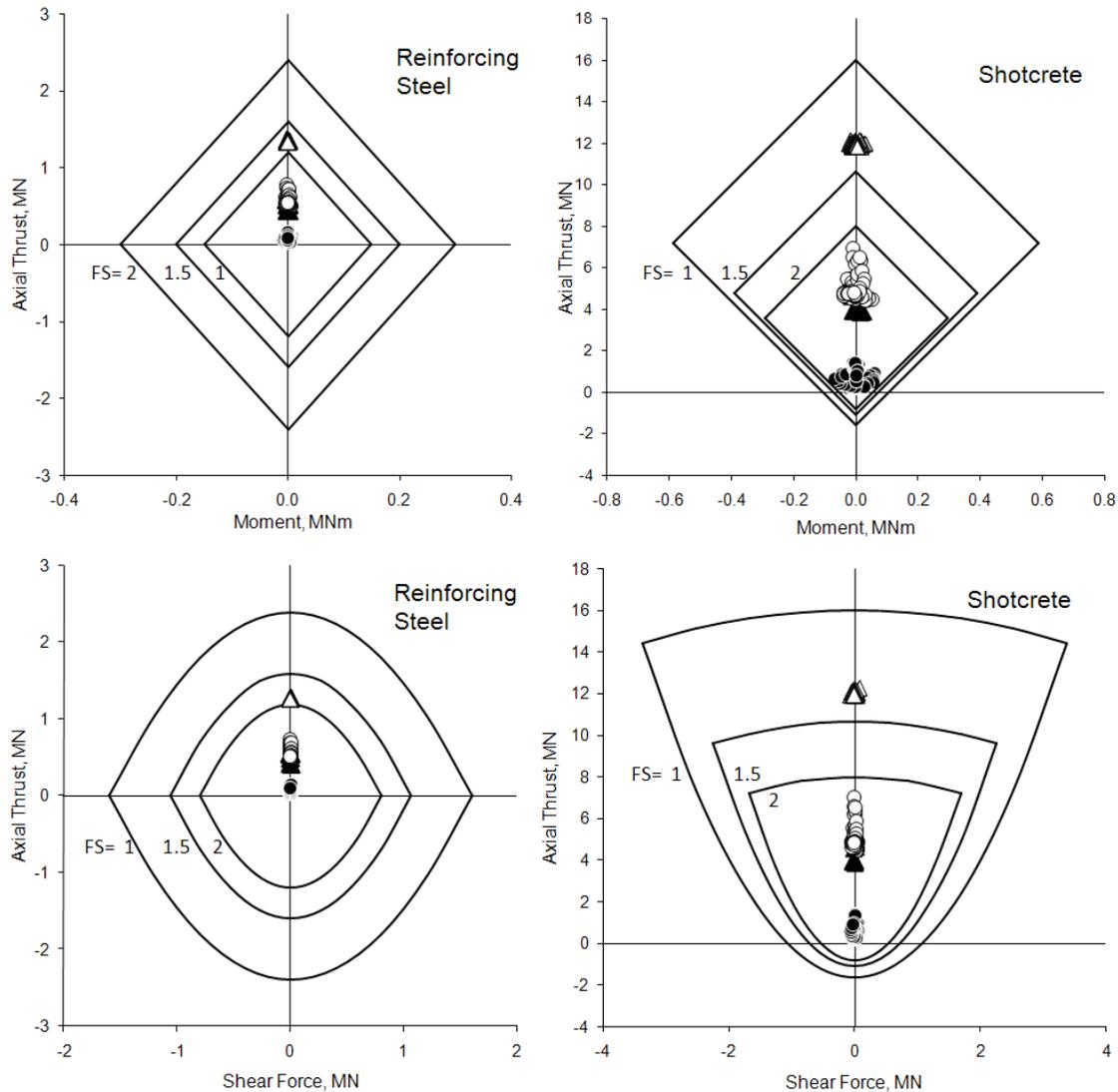
Figure 36. Partitioned liner loads compared to component capacity envelopes for full face tunnel option. Circles represent a full 60 cm lining, as per Figure 32b, installed in one step 2 m from the face. Triangles represent the option involving W 6x 20 sets installed at the face with a sliding gap in combination with 20 cm of shotcrete, followed at 10 m distance by a filled gap and 40 cm of reinforce shotcrete. These plots are for the inner 40 cm of reinforced shotcrete only. Filled symbols represent short term loading while open symbols are for long term loading.

The most obvious result from Figure 36 is the large axial thrust predicted in the full lining installed near the face with no sliding joints. This confirms the conclusion from Figure 29 and points to the definite requirement to allow deformation prior to full lining installation. For the full face excavation, the liner with a sliding joint and with the final reinforced layer applied at 10 m from the face performs well, giving a factor of safety for long term loading greater than 2 for all loading combinations. The limiting state is the short term moment in the shotcrete component (FS = 2). In this case the gap closed automatically in response to loading, between 5 and 10 m from the face, well before final lining installation.

As discussed, logistical and safety issues related to deformation and deterioration of the face mandated the adoption of a top heading and short bench sequence. This required the lining to be installed as an immediate top and slightly delayed bottom section. The partitioned capacity plots for top heading and bench excavation are shown in Figure 37.
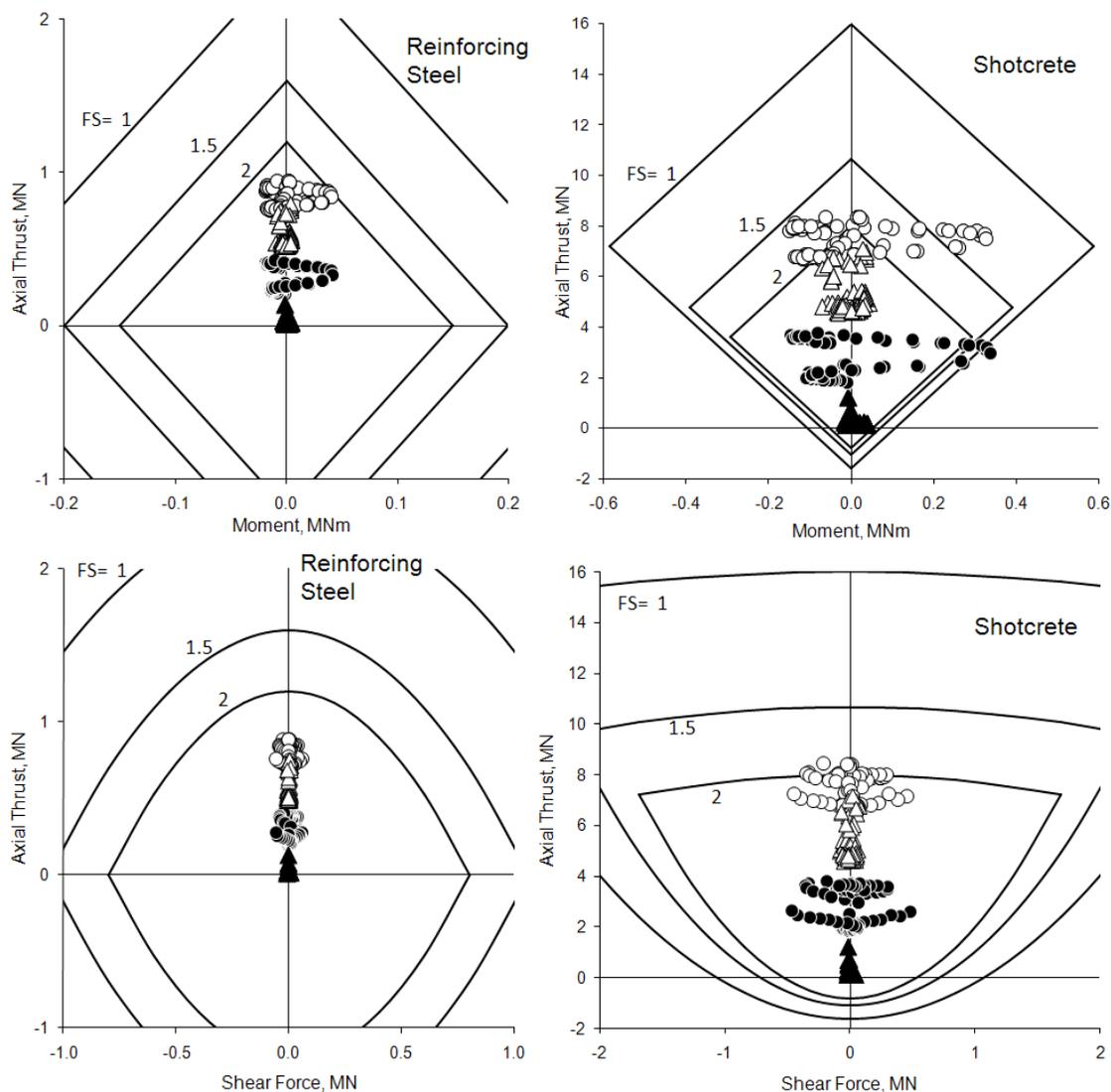
Figure 37. Partitioned liner loads compared to component capacity envelopes for top heading and bench options. In these analyses, the sliding joint (gap) closes automatically under load between 5 and 10 m. Circles represent completion of the final lining at 5 m from the face (before gap closure). Triangles represent the completion of the final lining at 10 m from the face (after gap closure). These plots are for the inner 40 cm of reinforced shotcrete only. Filled symbols represent short term loading while open symbols represent long term loading.

33

For the top heading and bench option, the predicted performance is adequate in short and long term loading provided that the gap (sliding joint) is filled and the final lining completed after the joint has fully closed or the deformations have stabilized. The penalty for delaying liner completion will be unacceptable degradation and yielding of the initial 20 cm lining and the steel sets resulting in service and safety problems. While this initial composite layer is expected to yield to some degree, excessive yielding should be avoided. In addition, a long delay in the installation of the final liner could lead to loss of wall control.

The ideal condition is to fill the gap with shotcrete immediately upon joint closure to complete the lining. In this example, the joint or gap closes between 6 m and 10 m from the face. The triangles in Figure 37 represent completion of the final liner at 10 m. The limiting state in this case is the short term moment in the shotcrete (FS > 2). The open circles in Figure 37 represent the case of premature completion of the final lining at 5 m from the face.

This design requires careful construction monitoring and management. If the gap is filled with shotcrete and the final lining competed before the joints are allowed to close or before deformations have stabilized, the penalty is increased axial, shear and moment loading throughout the liner. In the case shown here, cracking will be induced due to high moments for short term loading and the factor of safety for all loading combinations drops for long term loading.

Even with excellent construction management, however, it is possible that liner completion could take place too soon for some individual segments or rounds within the tunnel. From a hazard mitigation perspective it is important to understand the consequences of this possibility. The factors of safety illustrated in Figures 36 and 37 refer to initial cracking of the liner. Figure 38 illustrates an alternative analysis of the results in which the non-partitioned liner loadings and capacity envelopes are calculated in a non-linear fashion, using the program Response 2000 (Bentz, 2000) that allows plastic (cracked) moments.
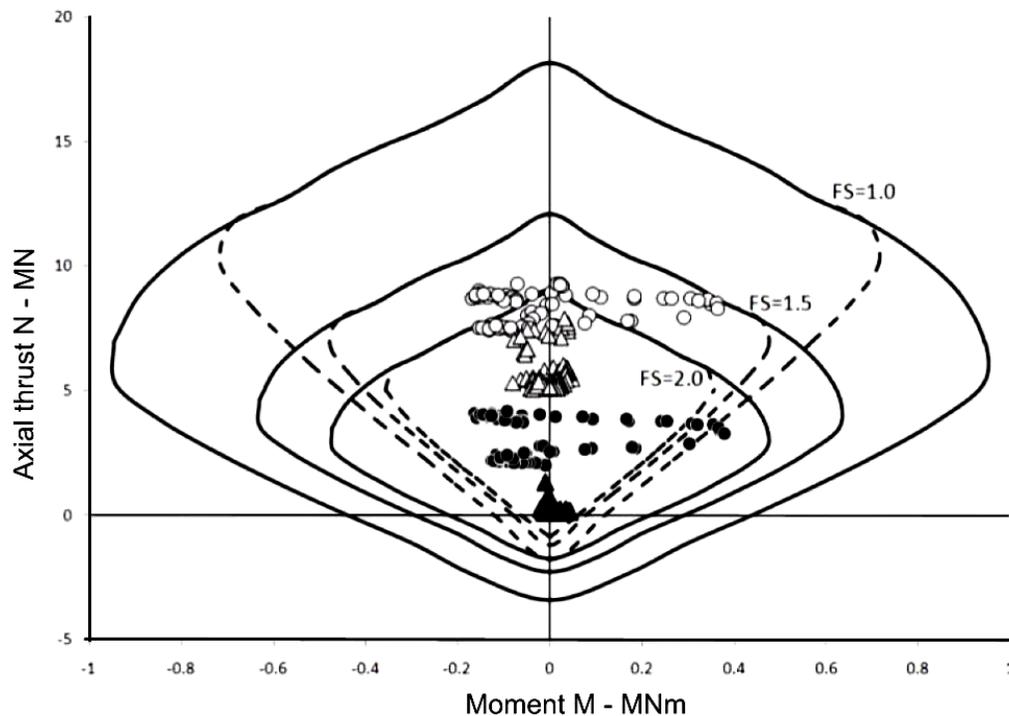
Figure 38. Total (non-partitioned) thrusts and moments from modeled inner liner of 40 cm reinforced shotcrete. Dashed envelopes represent limits for initial cracking of shotcrete. Solid envelopes represent capacity limits accounting for the development of additional moment capacity in the cracked liner as well as accounting for the tensile strength of the reinforcement (Vecchio and Collins, 1986). Triangles represent installation of the final lining at 10 m; circles represent completion at 5 m. Filled symbols indicate short term loading; open symbols indicate long term loading. Sliding joint closes automatically between 5 and 10 m from the face.

Figure 38 shows that the critical loading, in the case of premature completion of the liner, is the short term moment. This is indicated by the calculated values falling outside the capacity envelopes for cracking. These envelopes are equivalent to the elastic envelopes for the partitioned liner, presented in the previous figures. This case still falls within the solid capacity envelopes representing the ultimate load capacity of the liner with tension cracks fully developed and internal loading redistributed. This indicates that the prematurely installed final lining will not collapse catastrophically in compression or bending. Instead, cracks would become visible during the construction phase of the tunnel and repairs can be made.

The ultimate result is a reduced long term factor of safety for all loading conditions, again reinforcing the need for good construction management to ensure the correct installation sequence for potentially variable rock mass conditions and deformation rates.

The appearance of the tunnel, constructed as described in this example, is shown in Figure 39.

Figure 39. Completed section of tunnel with a 60 cm thick reinforced shotcrete lining, placed in two layers as described above.

4 CONCLUSIONS

A methodology for the design of tunnel linings has been presented. While this approach has been used by specialist tunnel designers for many years, it has never been described comprehensively in a single document that allows the reader to follow all the derivations and the step by step calculations. To make this process as easy as possible to follow, the authors have included two case history based examples, one for a very shallow tunnel and the other for a very deep tunnel. These examples have been chosen to highlight the complex loading conditions that can occur under different geological and topographic conditions and how these complexities can be incorporated into a rational lining design.

The support capacity diagrams are based on elastic analysis of the support elements and this implies that no tensile cracking or compressive crushing of the shotcrete or concrete elements is acceptable. These simplified calculations allow the user to optimize the design of the lining components relatively quickly and efficiently. It has been demonstrated that, where tensile cracking becomes an important consideration, more sophisticated non-linear structural design approaches, which allow for crack development, can be used.

5 ACKNOWLEDGEMENTS

6 SOFTWARE

The methodologies described in this paper can be used with any modern numerical package provided the input and verification of results are done according to equations and procedures presented. The three-dimensional analyses were carried out using FLAC3D, developed and sold by Itasca (www.itascacg.com) while all other calculations were performed using Phase2, developed and sold by Rocscience (www.rocscience.com).

The structural program *Response 2000*, developed by Professor Bentz, can be downloaded (free) from (http://www.ecf.utoronto.ca/~bentz/home.shtml).

7 REFERENCES

American Concrete Institute (2005). ACI 318-05. *Building Code Requirements for Structural Concrete*. Farmington Hills, Michigan.

Barton, N.R., Lien, R. and Lunde, J. 1974. Engineering classification of rock masses for the design of tunnel support. *Rock Mech.* **6**(4), 189-239.

Bentz, E.C., Sectional Analysis of Reinforced Concrete, *PhD Thesis*, Department of Civil Engineering, University of Toronto, 2000.

Bieniawski, Z.T. 1973. Engineering classification of jointed rock masses. *Trans S. Afr.Inst. Civ. Engrs* 15, 335-344.

British Tunnelling Society, 2004. *Tunnel lining design guide*. Thomas Telford, London.

Carranza-Torres, C., Fairhurst, C., 2000. Application of the convergence–confinement method of tunnel design to rock masses that satisfy the Hoek–Brown failure criterion. *Tunnelling Underground Space Technology* 15(2), 187–213

Carranza-Torres, C. and Diederichs, M.S. 2009 Mechanical analysis of a circular liner with particular reference to composite supports –e.g., liners consisting of shotcrete and steel sets, Submitted for review and publication to *Tunneling and Underground Space Technology* (Accepted and in press - Feb 2009.)

Chern, J.C., Shiao, F.Y., Yu, C.W. 1998. An empirical safety criterion for tunnel construction. *Proceedings of the Regional Symposium on Sedimentary Rock Engineering*, Taipei, Taiwan,. 222–227.

Duddeck, H. 1988. Guidelines for the Design of Tunnels. Prepared by the International Tunnelling Association Working Group on General Approaches to the Design of Tunnels. *Tunneling and Underground Space Technology*, 3(3). 237-249.

Guevara Briceño, R. 2004a. Túnel Yacambú-Quibor, Experiencia de Construcción - Reparación Tramo entre las Progresivas 12+800 a 12+950. In Sociedad Venezolana de Geotecnia (Ed.), *Actas del XVII Seminario Venezolano de Geotecnia.Geoinfraestructura: la Geotecnia en el Desarrollo Nacional*. Caracas, Venezuela. Noviembre, 2004.

Guevara Briceño, R. 2004b. Aspectos sobre diseño y construcción de los últimos 4.6 km del túnel de Yacambú. In Sociedad Venezolana de Geotecnia (Ed.), *Actas del XVII Seminario Venezolano de Geotecnia. Geoinfraestructura: la Geotecnia en el Desarrollo Nacional.* Caracas, Venezuela. Noviembre, 2004.

Hoek, E, 2001. Big tunnels in bad rock, 2000 Terzaghi lecture. *ASCE Journal of Gotechnical and Geoenvironmental Engineering*, 127(9), 726-740.

Hoek, E. and Marinos, P. 2000 Predicting Tunnel Squeezing. *Tunnels and Tunnelling International*. Part 1 – November 2000, Part 2 – December, 2000.

Hoek E., Carranza-Torres C., Corkum B. 2002 Hoek-Brown criterion – 2002 edition. *Proc. NARMS-TAC Conference*, Toronto, 2002, 267-273.

Hoek, E. 1992. When is a design in rock engineering acceptable ? - 1991 Müller lecture. *Proc. 7th Congress Intnl.. Soc. Rock Mech.*, Aachen. Rotterdam : A.A. Balkema.

Hoek, E. and Diederichs, M. S. 2006. Empirical estimation of rock mass modulus. *Int. J. Rock Mech. Min. Sci.* 43(2), 203–215.

Kaiser, P.K. 1985. Rational assessment of tunnel liner capacity. *Proc. 5th Canadian Tunnelling Conference.* Montreal.

Lunardi, P. 2000. The design and construction of tunnels using the approach based on the analysis of controlled deformation in rocks and soils. *Tunnels and Tunnelling International special supplement*, ADECO-RS approach, May 2000.

Marinos, P and Hoek, E. (2000) GSI – A geologically friendly tool for rock mass strength estimation. *Proc. GeoEng2000 Conference*, Melbourne. 1422-1442.

Melbye, T. and Garshol, K.F. 2000. *Spayed shotcrete for rock support.* Master Builders Technologies.

O'Rourke, T.D. 1984. *Guidelines for tunnel lining design*. Prepared by Technical Committee on Tunnel Lining Design of the Underground Technology Research Council, ACSE, New York.

Panet M. 1995. *Calcul des Tunnels par la Me´thode de Convergence–Confinement*. Presses de l'Ecole Nationale des Ponts et Chausse´es. Paris. 178p

Panet, M. 1993. Understanding deformations in tunnels. In: Hudson,J.A., Brown, E.T., Fairhurst, C., Hoek, E. (Eds.), *Comprehensive Rock Engineering*, Vol. 1. Pergamon, London, 663–690.

Panet, M. and Guenot, A. 1982. Analysis of convergence behind the face of a tunnel. *Proceedings, International Symposium Tunnelling'82*, IMM, London, 197–204.

Salcedo, D. 1983. Macizos Rocosos: Caracterización, Resistencia al Corte y Mecanismo de Rotura. *Proc. 25. Aniversario Conferencia Soc. Venezolana de Mecánica de Suelos e Ingeniería de Fundaciones*, Caracas. 143-172.

Sánchez Fernández, J.L. and Terán Benítez, C.E. 1994. Túnel de Trasvase Yacambú-Quibor. Avance Actual de los Trabajos de Excavación Mediante la Utilización de Soportes Flexibles Aplicados a Rocas con Grandes Deformaciones. *Proc. IV Congreso Sudamericano de Mecanica de Rocas, Santiago* 1, 489-497.

Schubert, W. 1996. Dealing with squeezing conditions in Alpine tunnels. *Rock Mech. Rock Engrg*. **29**(3), 145-153.

Sauer, G., Gall, V. Bauer, E and Dietmaier, P. 1994. Design of tunnel concrete linings using limit capacity curves. in *Computer Methods and Advances in Geomechanics*, Eds.: Siriwardane & Zaman, Rotterdam, NL. 2621 – 2626.

Unlu, T. and Gercek, H. 2003. Effect of Poisson's ratio on the normalized radial displacements occurring around the face of a circular tunnel. *Tunnelling and Underground Space Technology.* **18**. 547–553

Vecchio, F.J., and Collins, M.P., 1986. The Modified Compression Field Theory for Reinforced Concrete Elements Subjected to Shear, *ACI Journal*, **83**(2), 219-231

Vlachopoulos, N. and Diederichs, M.S. 2009a. Improved longitudinal displacement profiles for convergence-confinement analysis of deep tunnels. *Rock Mechanics and Rock Engineering* (Accepted - In Press) 16 pgs.

Vlachopoulos, N. and Diederichs, M.S. 2009b. Comparison of 2D and 3D analysis methods forsingle and paired tunnels in weak highly stressed ground. Paper to be submitted to *Tunnels and Underground Space Technology.* 40 manuscript pages.

8 APPENDIX 1 – CALCULATION OF LONGITUDINAL DISPLACEMENT PROFILES

In order to design the appropriate timing for the installation of stiff support or when optimizing the installation of support with specific displacement capacity, it is important to determine the longitudinal closure profile for the tunnel. A portion of the maximum radial displacements at the tunnel boundary will take place before the face advances past a specific point. The tunnel boundary will continue to displace inwards as the tunnel advances further beyond the point in question. This longitudinal profile of closure or displacement versus distance from the tunnel face is called the longitudinal displacement profile and can be calculated using three-dimensional models for complex loading and geometric conditions or with axisymmetric models for uniform or isotropic initial stress conditions and circular tunnel cross sections. This profile can be used to establish a distance-convergence relationship for 2D modeling or for analytical solutions (as in Carranza-Torres and Fairhurst, 2000). The following discussion of longitudinal displacement profile estimation is excerpted from Vlachopoulos and Diederichs (2009a).

In order to facilitate analytical calculations of ground response (convergence-confinement) Panet (1995) derived a relationship for the longitudinal displacement profile based on elastic analysis:

$$\frac{u_r}{u_{\max}} = \frac{1}{4} + \frac{3}{4}\left(1 - \left(\frac{3}{3+4d_t}\right)^2\right) \tag{A1.1}$$

where $d_t = X / R_t$, u_r is the average radial displacement at a specified longitudinal position, X, and u_{max} is the maximum short term radial displacement distant from the face and corresponding to plane strain analysis of a tunnel cross section. R_t is the tunnel radius and X is positive into the tunnel away from the face ($X = 0$). The position X is negative into the rock ahead of the face and is specified along the tunnel centerline.

Numerous other authors have suggested alternative expressions for the elastic longitudinal displacement profile including Unlu and Gercek (2003) who noted that the curve in front of the face and the curve behind the face do not follow a single continuous functional relationship with X. The radial deformation profile with respect to distance from the face is accurately predicted for the elastic case to be:

for X < 0;

$$\frac{u_r}{u_{\max}} = \frac{u_0}{u_{\max}} + A_a\left(1 - e^{B_a d_t}\right)$$

for X > 0

$$\frac{u_r}{u_{\max}} = \frac{u_0}{u_{\max}} + A_b\left(1 - \left(B_b /(A_b + d_t)\right)^2\right) \tag{A1.2}$$

where u_0 is the radial displacement at the face location ($X=0$) and A_a, A_b, B_a, B_b are functions of Poisson's Ratio:

$$\frac{u_0}{u_{\max}} = 0.22v + 0.19;$$

$$A_a = -0.22v - 0.19; \ B_a = 0.73v + 0.81 \tag{A1.3}$$

$$A_b = -0.22v + 0.81; \ B_b = 0.39v + 0.65$$

These preceding equations are for elastic deformation. Panet (1993, 1995), Panet and Guenot (1982), Chern et al. (1998) and other have proposed empirical solutions for longitudinal displacement profiles based on plastic modeled deformation of varying intensity (correlated to various indices such as the ratio between insitu stress and undrained cohesive strength, for example).

Alternatively, an empirical best fit to actual measured closure data can be used (for example – based on data from Chern et al, 1998):

$$\frac{u_r}{u_{max}} = \left(1 + e^{\left(\frac{-d_t}{1.10}\right)}\right)^{-1.7} \tag{A1.4}$$

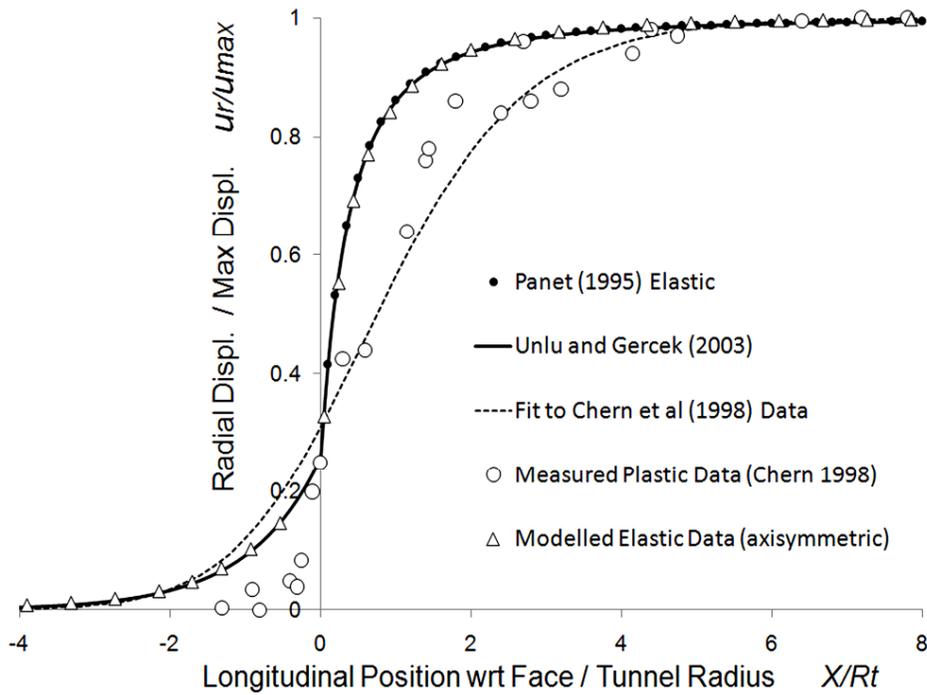These relationships are summarized in Figure A1.1.

Figure A1.1: Longitudinal displacement profile functions from various researchers and example data from Chern et al.(1998).

The development of radial deformation, however, is directly linked to the development of the plastic zone as the tunnel advances. Studies by the authors have shown that the longitudinal displacement profile function proposed by Panet (1995) and by Unlu and Gercek (2003) is reasonable for plastic analysis provided that the radius of the plastic zone does not exceed 2 tunnel radii and provided that the yielding zone in the tunnel face does not interact with the developing yield zone around the tunnel walls as illustrated in Figure A1.2.

The advancing front of plastic yielding is bullet shaped in three dimensions and for large plastic zones (radius of plastic zone $R_p \gg 2$) the shape of this developing yield zone is geometrically similar for increasing maximum plastic radii. There is no reason, therefore to expect that a single longitudinal displacement profile will suffice for these conditions. In order to account for the influence of increased overall yielding on the shape of the normalized longitudinal displacement profile, the most logical index to relate to the longitudinal displacement profile function is the ultimate radius of the normalized plastic zone radius, R_p/R_t.
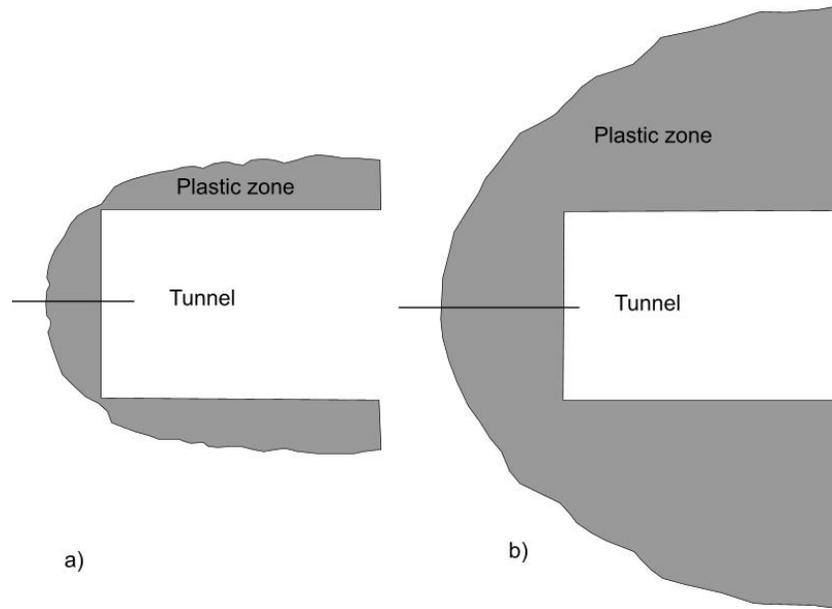
Figure A1.2: a) Plastic yield zone developing as tunnel advances to the left. Maximum plastic zone radius is less than twice the tunnel radius and the wall yield zone does not interact with the face yield zone (Panet's 1995 longitudinal displacement profile is valid); b) wall yield zone more than double the tunnel radius and interacts with face yield zone (Panet's longitudinal displacement profile is not valid).

To illustrate this problem, one series of analyses were performed involving a radial tunnel section and an axi-symmetric analysis along the tunnel axis. The first suite of analyses is based on a typical rock mass at 1100m depth in graphitic phyllite found in the Yacambu-Quibor Tunnel in Venezuela. This is case A_1 in the table below. In this case the initial insitu stress is approximately 10 times the estimated rock mass uniaxial strength. 5 other rock masses are investigated with increasing strength (increasing intact strength and/or GSI) giving a series of representative cases with varying po/σ_{crm} (in situ stress/rock mass strength). The rock mass parameters are summarized in Table A1.1.

Table A1.1: Rockmass parameters for longitudinal displacement profile analysis using PHASE2 (constant P_0=28MPa)

	A_1	B_1	C_1	D_1	E_1	F_1	G_1
P_0/σ_{crm}	10	8	6	4	2	1	Elastic
σ_{ci} (MPa)	35	35	35	50	75	100	
mi	7	7	7	7	7	7	
ν	0.25	0.25	0.25	0.25	0.25	0.25	
GSI	25	35	45	48	60	74	
m	0.481	0.687	0.982	1.093	1.678	2.766	
s	0.0002	0.0007	0.0022	0.0031	0.0117	0.0536	
a	0.531	0.516	0.508	0.507	0.503	0.501	
E_{rm} (MPa)	1150	2183	4305	7500	11215	27647	1150
σ_{crm}(MPa)	2.8	3.5	4.7	7	14	28	
P_0 (MPa)	28	28	28	28	28	28	28
Radius, m	2.5	2.5	2.5	2.5	2.5	2.5	2.5

The rock mass strengths are estimated as per Hoek et al (2002) and the elastic moduli are estimated based on Hoek and Diederichs (2007). A second set of analyses were performed based on rock mass A_1 (plastic) and G_1 (elastic) in Table A1.1 the stress levels listed in Table A1.2:

Table A1.2: Rockmass parameters for longitudinal displacement profile analysis using PHASE2 (constant σ_{crm}=2.8MPa)

	A_2	B_2	C_2	D_2	E_2	F_2	G_2
P_0/σ_{crm}	10	8	6	4	2	1	elastic
P_0 (MPa)	28	22.4	16.8	11.2	5.6	2.8	28

The tunnels were analyzed (with Phase2) in plane strain cross section to determine the extent of the plastic zone and the maximum radial deformation in each case. In addition, the cases were analyzed, using axisymmetric models, with 1 m incremental advance to determine the longitudinal displacement profile in each case as shown in Figure A1.3. The maximum displacements and sizes of plastic zone were comparable between the radial and longitudinal models. These summary results are presented in Table A1.3 and the resultant normalized longitudinal displacement profiles are presented in Figure A1.4.
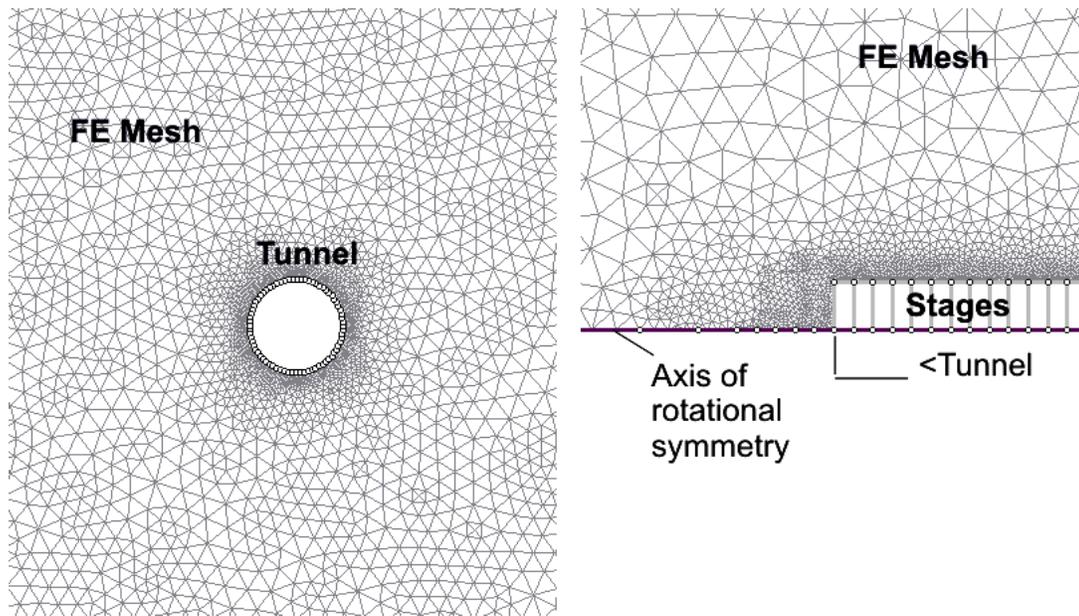

Figure A1.3: (left) radial tunnel section for PHASE2 analysis; (right) axisymmetric model with 1 m excavation stages (tunnel advances to the left).

Table A1.3: Summary results from radial and longitudinal (axisymmetric) analysis.

P_0/σ_{crm}	10	8	6	4	2	1	Elastic
Constant P_o	A_1	B_1	C_1	D_1	E_1	F_1	G
Plastic R_p	7.5	5.1	3.5	2.3	1.5	1.2	1
Max Disp	2.14	0.571	0.154	0.0495	0.0148	0.00367	0.0753
Constant σ_{crm}	A_2	B_2	C_2	D_2	E_2	F_2	G
Plastic R_p	7.5	6.3	5.0	3.3	2.2	1.6	1
Max Disp	2.14	1.25	0.632	0.242	0.0585	0.00167	0.0753
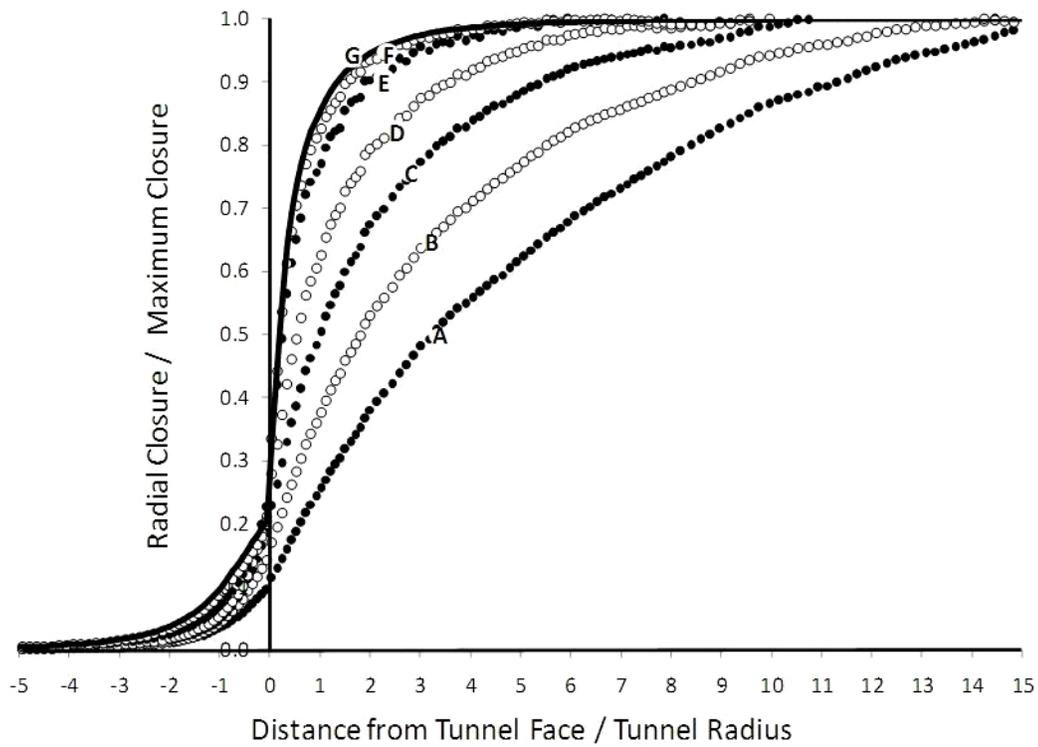
Distance from Tunnel Face / Tunnel Radius

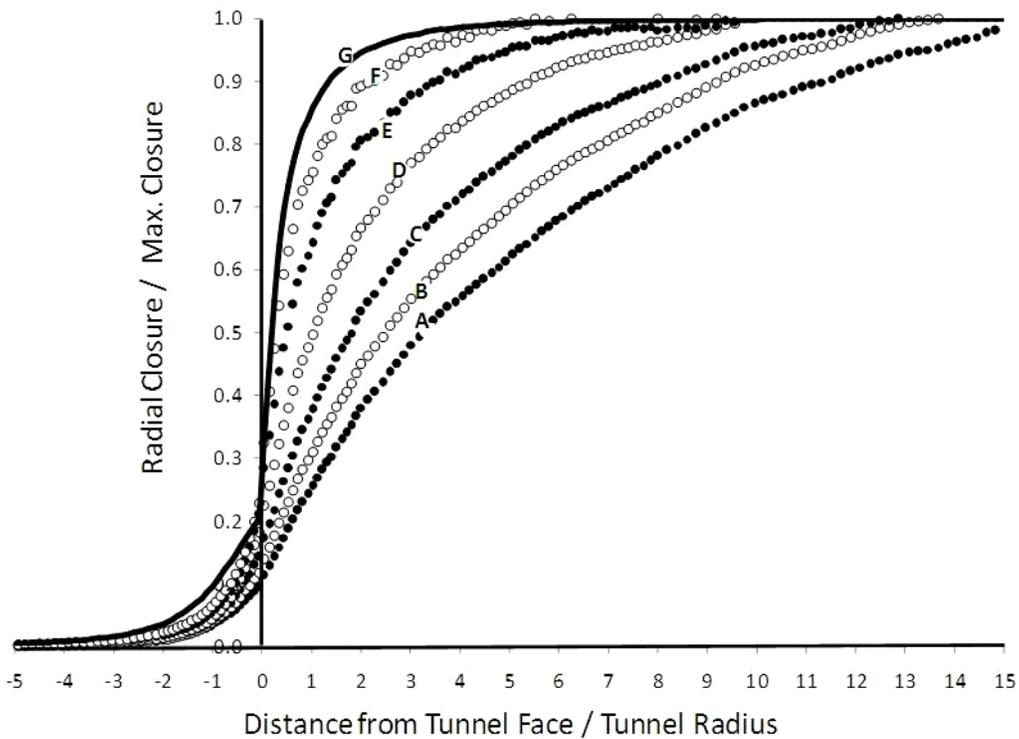Figure A1.4: Modeled longitudinal displacement profile results for axisymmetric models: (top) constant Po model results; (bottom) constant σ_{crm} model. Labeled results (A-G) correspond to models in Table A1.3.

By inspection of Figure A1.4 it is evident that the longitudinal displacement profile does not correlate with the stress/strength index P_0/σ_{crm} as the set of curves in both plots represent the same selected values for this ratio and yet have different longitudinal displacement profiles. Analysis of the data, however, shows a direct correlation with the maximum normalized plastic zone, R_p/R_t, as expected. The correlation between u_0/u_{max} at $X/R_t = 0$ (at the face) and the maximum plastic radius, R_p/R_t, is shown in Figure A1.5. Ignoring the influence of Poisson's ratio (negligible compared to plastic yielding) the best fit relationship (independent of material parameters and stress levels) is:

$$\frac{u_0}{u_{max}} = \frac{1}{3}e^{-0.15P_r} \tag{A1.5}$$
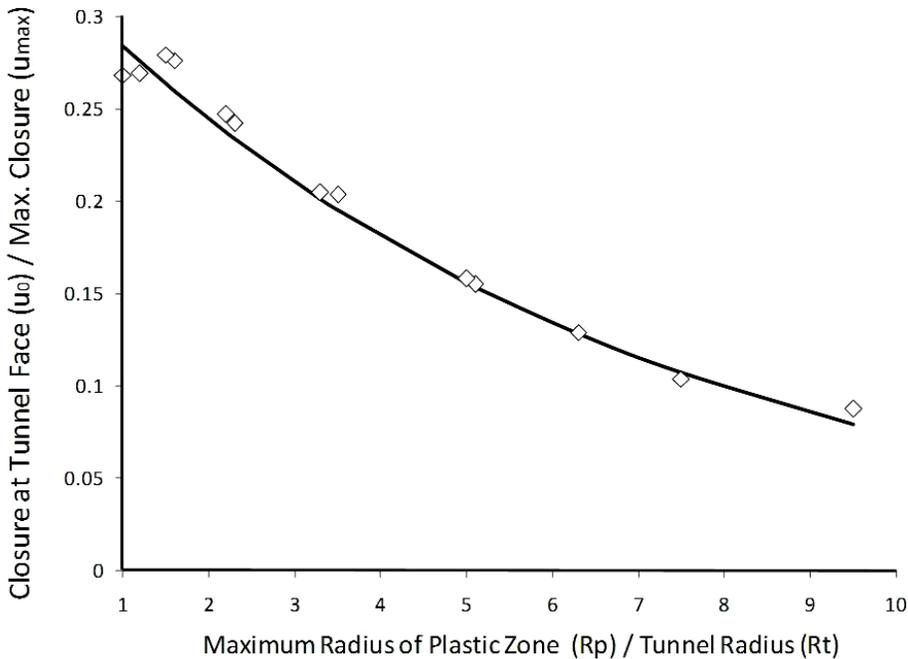
where $P_r = R_p / R_t$

Figure A1.5: Correlation between u_0/u_{max} at $X/R_t = 0$ (at the face) and the maximum plastic radius, R_p/R_t for analyses in table A1.4.

The relationships proposed by Unlu and Gercek (2003) correctly illustrate that the behavior ahead of the face (X<0 into the rockmass) does not follow the same continuous function as the behavior (progressive displacement) behind the face (X>0 in the tunnel). Their functions summarized in Equation A1.2, do not, however, capture the influence of a large developing plastic zone.

Based on the analysis in the preceding discussion, a new set of relationships are presented here that capture the influence of large plastic zone development on the longitudinal displacement profile. Equation A1.5 gives the relationship between normalized plastic radius and normalized closure at the face (X=0). Equations A1.6 and A1.7 give the best fit longitudinal displacement profile for X<0 and X>0 as a function of normalized maximum plastic zone radius.
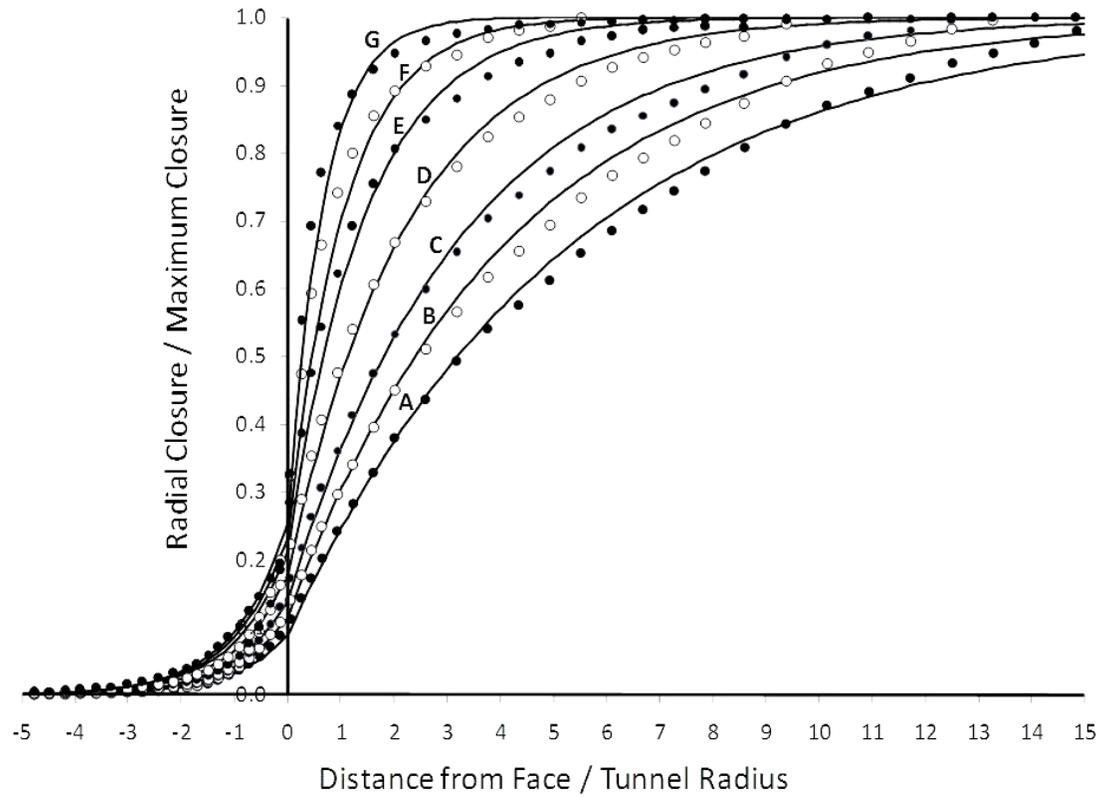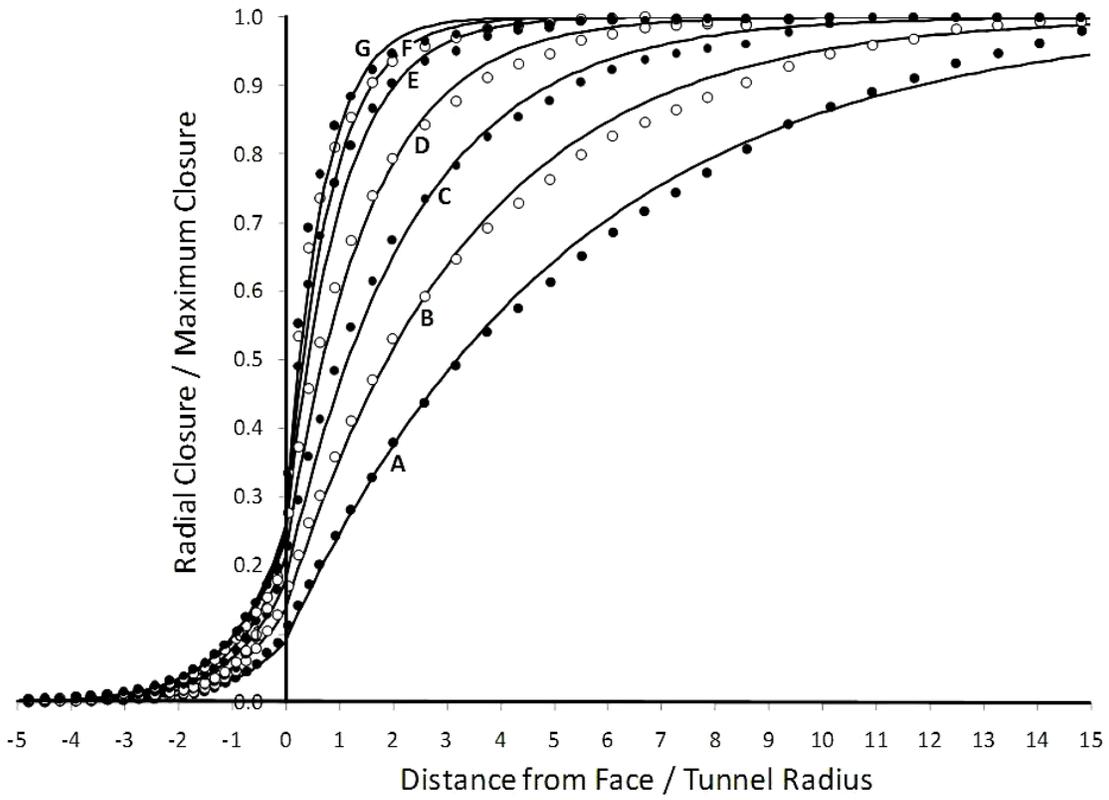
Figure A1.6: Correlation between predicted longitudinal displacement profiles (Equations A1.6 and A1.7) and model data (analyses from Table A1.4). (top) constant p_0 analysis; (bottom) constant σ_{crm} analysis.

The correlation with model data is shown in Figure A1.6.

$$\frac{u}{u_{\max}} = \frac{u_0}{u_{\max}} \cdot e^{d_t} \qquad \text{for X} < 0 \text{ (in the rock mass)} \tag{A1.6a}$$

$$d_t = \ln\left(\frac{u}{u_0}\right) \qquad \text{for} \quad u < u_0 \tag{A1.6b}$$

where u_0/u_{max} is given by Equation A1.5.

$$\frac{u}{u_{\max}} = 1 - \left(1 - \frac{u_0}{u_{\max}}\right) \cdot e^{-\frac{3d_t}{2P_r}} \qquad \text{for X} > 0 \text{ (in the tunnel).} \tag{A1.7a}$$

$$d_t = -\frac{2}{3}P_r \ln\left(\frac{u_{\max} - u}{u_{\max} - u_0}\right) \quad \text{for} \quad u > u_0 \tag{A1.7b}$$

There is an important caveat to consider when using numerical analysis to compute longitudinal displacement profiles. When using axisymmetric or full three-dimensional models to determine the longitudinal displacement profile relationship, it is important to consider the excavation rate. A stress front builds ahead of the bullet shaped plastic zone and influences the rate of plastic zone development. Such models will yield a different apparent longitudinal displacement profile depending on the size of the excavation step. This is clearly shown in Figure A1.7, where there is a significant difference between the instantaneous excavation and the 1m (0.2D) step simulation (other excavation step sizes shown for comparison). For support sequencing it is important to simulate the actual excavation step size or, if the tunneling is continuous (TBM), to use a small step size.
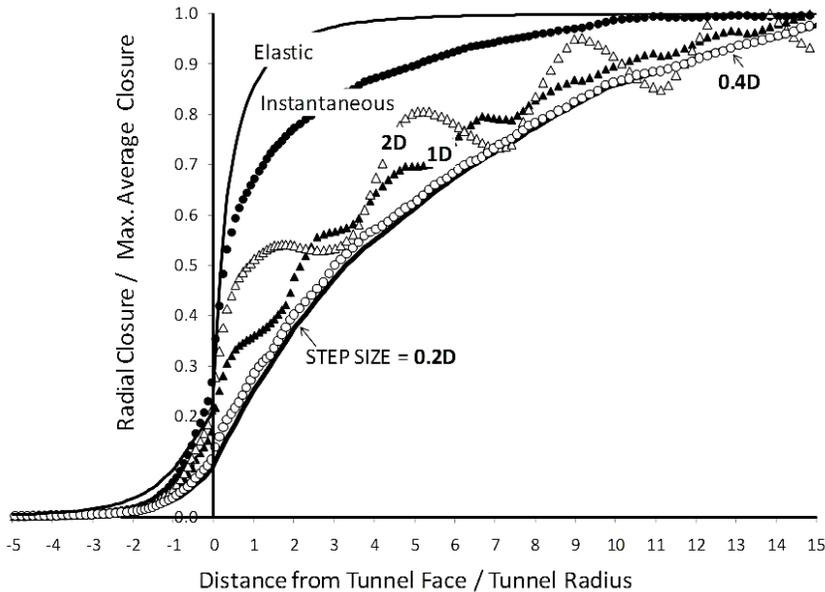

Figure A1.7: Influence of excavation step size on the longitudinal displacement profile.

46

9 APPENDIX 2 - MOMENTS AND FORCES IN LINING ELEMENTS

In a typical tunnel design in which support consists of steel sets embedded in shotcrete, the designer needs to know the contribution of each of these support elements and to be able to adjust the number and dimensions of each to accommodate the loads imposed on the lining. In current tunnel design, these loads are obtained from numerical analyses in which "beam elements" are attached to the tunnel boundary and the axial thrust, bending moments and shear forces induced in these elements are computed directly.

Note that these beam elements constitute "tunnel support" and they interact with the surrounding rock mass to limit the convergence of the tunnel. On the other hand, rockbolts act as "tunnel reinforcement" in that they change the mechanical properties of the rock mass surrounding the tunnel. Hence, it is possible to carry out a numerical analysis of a tunnel reinforced by means of rockbolts and supported by means of a composite lining. The loads imposed on the lining will be reduced by the reinforcement and the composite lining will respond to these reduced loads. The analysis that follows is valid whether rockbolts are present or not, provided that the numerical analysis correctly models the load transfer from the rock mass onto the lining.

Figure A2.1 represents the problem to be analyzed involving a section of composite liner of width b comprising n steel sets and n units of shotcrete —note that if n units of each material exist along the width b, this is equivalent to saying that the units are spaced at $s = b/n$. The composite section in Figure 1 can be regarded as an equivalent section of width b and thickness t_{eq}. The steel sets are assumed to be symmetrically placed in the shotcrete lining so that the neutral axes of both the steel sets and the shotcrete lining are coincident. For the purposes of this analysis it is assumed that the complete shell behaves elastically. This is a reasonable assumption since the tunnel designer generally attempts to design the lining so that it will not fail.

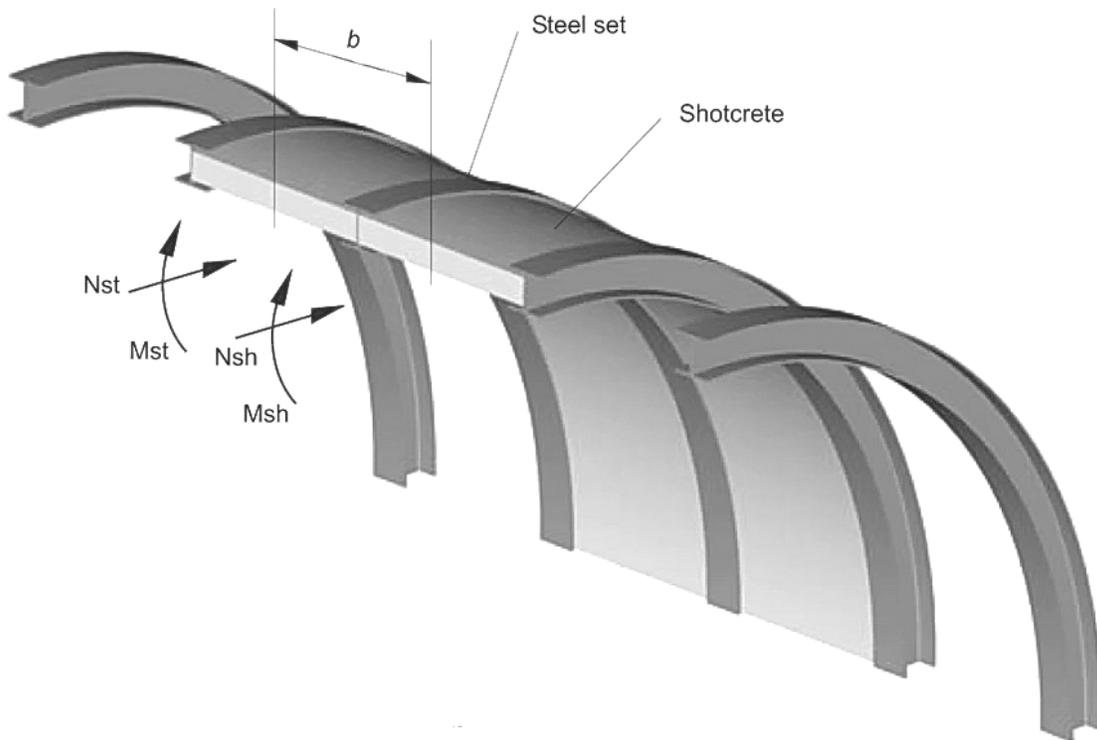The following analysis is excerpted from Carranza-Torres and Diederichs (2009).

Figure A2.1: A section of width b in a composite lining consisting of steel sets, spaced at a distance s, embedded in shotcrete. Moments M_{st} and axial thrusts N_{st} are induced in the steel sets and moments M_{sh} and thrusts N_{sh} are induced in the shotcrete shell.

In order to calculate the moments and axial thrusts induced in the steel sets and the shotcrete shell and to compare these with the capacity of the steel sets and shotcrete, the following steps are required:

1. An "equivalent" rectangular section with a width of b, a thickness t_{eq} and a modulus of E_{eq}, is determined.
2. The capacity of the steel sets and the shotcrete lining are determined.
3. A numerical model of the tunnel is constructed and beam elements representing the equivalent rectangular section are applied to the tunnel perimeter.
4. The bending moments and axial thrusts are redistributed back onto the steel sets and shotcrete lining.

9.1 *Calculation of equivalent section*

The properties of the equivalent rectangular section are calculated as follows. For plane strain conditions the compressibility coefficient D_{st} and flexibility coefficient K_{st} for the steel sets are:

$$D_{st} = \frac{E_{st} A_{st}}{1 - v_{st}^2} \tag{A2.1}$$

$$K_{st} = \frac{E_{st} I_{st}}{1 - v_{st}^2} \tag{A2.2}$$

where E_{st} is the Young's modulus of the steel
 A_{st} is the cross-sectional area of each steel set
 I_{st} is the moment of inertia of each steel set and
 v_{st} is the Poisson's ratio of the steel

For the shotcrete shell, the compressibility and flexibility coefficients are:

$$D_{sh} = \frac{E_{hst} A_{sh}}{1 - v_{sh}^2} \tag{A2.3}$$

$$K_{sh} = \frac{E_{sh} I_{sh}}{1 - v_{sh}^2} \tag{A2.4}$$

where E_{sh} is the Young's modulus of the shotcrete
 A_{sh} is the cross-sectional area of each unit of shotcrete $= s.t_{sh}$
 I_{sh} is the moment of inertia of each unit of shotcrete $= (s.t_{sh}^3)/12$
 v_{sh} is the Poisson's ratio of the shotcrete

The equivalent compressibility and flexibility coefficients for the composite lining are:

$$D_{eq} = n(D_{st} + D_{sh}) \tag{A2.5}$$

$$K_{eq} = n(K_{st} + K_{sh}) \tag{A2.6}$$

The equivalent section has a width of b, an equivalent section thickness t_{eq} and the equivalent modulus E_{eq}. The equivalent compressibility and flexibility coefficients can be written as:

$$D_{eq} = b.t_{eq} E_{eq} \tag{A2.7}$$

$$K_{eq} = E_{eq} \frac{b.t_{eq}^3}{12} \tag{A2.8}$$

Solving for the variables t_{eq} and E_{eq}

$$t_{eq} = \sqrt{\frac{12 K_{eq}}{D_{eq}}} \tag{A2.9}$$

$$E_{eq} = \frac{D_{eq}}{b t_{eq}} \tag{A2.10}$$

9.2 *Calculation of support capacity*

In order to check whether the induced stresses in the steel sets and shotcrete lining are within permissible limits, it is useful to plot the moments, shear forces and thrusts on support capacity diagrams. The support capacity curves are calculated as follows:

9.2.1 *Moment-thrust capacity*

The maximum permissible compressive and tensile stresses induced in the lining are given by:

$$\frac{\sigma_{max}}{FS} = \frac{N}{A} + \frac{Mt}{2I} \tag{A2.11}$$

$$\frac{\sigma_{min}}{FS} = \frac{N}{A} - \frac{Mt}{2I} \tag{A2.12}$$

where FS is the factor of safety.

The maximum and minimum permissible thrust capacity is obtained by substituting $M = 0$ in equations A2.11 and A2.12, giving:

$$N_{max} = \frac{A\sigma_{max}}{FS} \tag{A2.13}$$

$$N_{min} = \frac{A\sigma_{min}}{FS} \tag{A2.14}$$

The maximum bending moment is obtained when tensile and compressive failures occur simultaneously which, by eliminating N from equations A2.11 and A2.12, gives:

$$M_{max} = \pm \left(\frac{\sigma_{max} - \sigma_{min}}{FS} \right) \frac{I}{t} \tag{A2.15}$$

The corresponding normal force N_{cr} at which these maximum moments occur is given by:

$$N_{cr} = \frac{A(\sigma_{max} + \sigma_{min})}{2FS} \tag{A2.16}$$

9.2.2 *Shear force-thrust capacity*

In terms of shear force and axial thrust relationships:

$$\sigma_{max} = \frac{N}{A} \qquad (A2.17)$$

$$\tau_{max} = \frac{3Q}{2A} \qquad (A2.18)$$

$$\sigma_{1,3} = \frac{\sigma_{max}}{2} \pm \sqrt{\left(\frac{\sigma_{max}}{2}\right)^2 + \tau_{max}^2} \qquad (A2.19)$$

$$FS = \frac{\sigma_c}{\sigma_1} = \frac{\sigma_t}{\sigma_3} \qquad (A2.20)$$

For failure in compression: $\quad N = \dfrac{\sigma_c A}{FS} - \dfrac{9Q^2 FS}{4\sigma_c A} \qquad (A2.21)$

For failure in tension: $\quad N = \dfrac{\sigma_t A}{FS} - \dfrac{9Q^2 FS}{4\sigma_t A} \qquad (A2.22)$

The critical value of the shear force Q_{cr} associated with a particular factor of safety FS for both failure in compression and tension at the same time is:

$$Q_{cr} = \pm \frac{A}{FS} \sqrt{-\frac{4\sigma_c \sigma_t}{9}} \qquad (A2.23)$$

Note that σ_t is negative.

9.3 *Redistribution of thrust and moment onto steel sets and shotcrete*

The bending moments, shear forces and axial thrusts are calculated by means of a numerical analysis and for the equivalent composite lining of width b and thickness t_{eq}. In order to consider the behavior of the steel sets and the shotcrete separately, it is necessary to redistribute these thrusts and moments back onto the individual support elements.

Since many of the linings are attached to curved surfaces and, in some cases, these linings are relatively thick compared to their radius R, it is necessary to consider the redistribution in terms of a thick curved beam solution. This solution is the most general since it automatically degenerates to a thin beam solution as the radius of curvature increases to infinity.

The equations for the redistribution of the moment M, axial thrust N and shear forces Q induced in any one of the beam elements representing the equivalent shell are:

Steel set moments: $\quad M_{st} = \dfrac{MK_{st}}{n(K_{st} + K_{sh})} \qquad (A2.24)$

Shotcrete moments: $\quad M_{sh} = \dfrac{MK_{sh}}{n(K_{st} + K_{sh})} \qquad (A2.25)$

Steel set thrusts: $\quad N_{st} = \dfrac{N.D_{st}}{n(D_{st} + D_{sh})} + \dfrac{M(D_{sh}K_{st} - D_{st}K_{sh})}{nR(D_{st} + D_{sh})(K_{st} + K_{sh})} \qquad (A2.26)$

$$N_{st} = \frac{N.D_{sh}}{n(D_{st} + D_{sh})} - \frac{M(D_{sh}K_{st} - D_{st}K_{sh})}{nR(D_{st} + D_{sh})(K_{st} + K_{sh})}$$

Shotcrete thrusts: (A2.27)

$$Q_{st} = \frac{QK_{st}}{n(K_{st} + K_{sh})}$$

Steel set shear forces: (A2.28)

$$Q_{sh} = \frac{QK_{sh}}{n(K_{st} + K_{sh})}$$

Shotcrete shear forces: (A2.29)

9.4 Support capacity plots

The capacity plots described above can be calculated by means of a simple spreadsheet. The following input parameters have been assumed for this analysis:

Steel sets		*Shotcrete lining*	
Tunnel radius	$R = 2$ m	Shotcrete thickness	$t_{sh} = 0.2$ m
Steel set spacing	$s = 0.6$ m	Modulus of shotcrete	$E_{sh} = 30,000$ MPa
Steel set height	$t_{st} = 0.162$ m	Poisson's ratio	$v_{sh} = 0.15$
Area of steel set	$A_{st} = 4.75 \times 10^{-3}$ m^2	Compressive strength	$\sigma_{csh} = 40$ MPa
Moment of Inertia	$I_{st} = 2.23 \times 10^{-5}$ m^4	Tensile strength	$\sigma_{tsh} = -2.5$ MPa
Modulus of steel	$E_{st} = 200,000$ MPa	Area of shotcrete	$A_{sh} = s.t_{sh} = 0.12$ m^2
Poisson's ratio	$v_{st} = 0.25$	Moment of Inertia	$I_{sh} = s.t_{sh}^3/12 = 0.0004$ m^4
Compressive strength	$\sigma_{cst} = 500$ MPa		
Tensile strength	$\sigma_{tst} = -500$ MPa		

Calculation of Support capacity diagrams for a Factor of Safety = 1.0

Steel sets	M	N	*Shotcrete lining*	M	N
Maximum Thrust	0.00	2.38	Maximum Thrust	0.00	4.80
Maximum moment	0.14	0.00	Maximum moment	0.09	2.10
Minimum thrust	0.00	-2.38	Minimum thrust	0.00	-0.60
Minimum moment	-0.14	0.00	Minimum moment	-0.09	2.10
Complete fig	0.00	2.38	Complete fig	0.00	4.80

Shear force - axial thrust plot

Steel sets	Q	N	N	Shotcrete lining	Q	N	N
Maximum shear force	1.58			Maximum shear force	1.13		
Minimum shear force	-1.58			Minimum shear force	-1.13		
	1.58	0.00	0.00		1.13	4.20	4.20
	1.19	1.04	-1.04		0.85	4.46	2.10
	0.79	1.78	-1.78		0.57	4.65	0.60
	0.40	2.23	-2.23		0.28	4.76	-0.30
	0.00	2.38	-2.38		0.00	4.80	-0.60
	-0.40	2.23	-2.23		-0.28	4.76	-0.30
	-0.79	1.78	-1.78		-0.57	4.65	0.60
	-1.19	1.04	-1.04		-0.85	4.46	2.10
	-1.58	0.00	0.00		-1.13	4.20	4.20

The following forces induced in the lining described above are redistributed into the steel and shotcrete components as defined by Equations A2.24 to A2.29. The lining was installed in a circular tunnel with a radius of 5 m in a rock mass with properties defined by:

Modulus E = 4000 MPa
Peak cohesion = 2 MPa, Residual cohesion = 1 MPa
Peak friction angle = 40°, Residual friction angle = 35°

The rock mass is subjected to a horizontal stress normal to the tunnel axis of 4 MPa and a vertical stress of 2 MPa. The horizontal stress parallel to the tunnel axis is 2 MPa.

The results of these calculations are plotted in Figure A2.2.

Redistribution of forces into steel and shotcrete lining components (Equations A2.24 to A2.29)

| Total M	Total Q	Steel N	Steel M	Steel Q	Shot N	Shot M	Shot Q
0.00692	0.00242	0.40880	0.00121	0.00042	1.39360	0.00294	0.00103
0.00591	0.00049	0.43527	0.00103	0.00009	1.48383	0.00251	0.00021
0.00451	0.00371	0.49292	0.00079	0.00065	1.68034	0.00192	0.00158
0.00266	0.00206	0.57431	0.00047	0.00036	1.95781	0.00113	0.00088
-0.00057	-0.00719	0.67026	-0.00010	-0.00126	2.28492	-0.00024	-0.00305
-0.00283	-0.00224	0.77803	-0.00050	-0.00039	2.65229	-0.00120	-0.00095
-0.00518	0.00738	0.86640	-0.00091	0.00129	2.95356	-0.00220	0.00313
-0.00632	-0.00213	0.91111	-0.00111	-0.00037	3.10595	-0.00269	-0.00091
-0.00680	0.00133	0.91191	-0.00119	0.00023	3.10869	-0.00289	0.00057
-0.00519	-0.00831	0.86533	-0.00091	-0.00146	2.94989	-0.00221	-0.00353
-0.00315	-0.00787	0.79319	-0.00055	-0.00138	2.70397	-0.00134	-0.00334
-0.00121	-0.00529	0.70242	-0.00021	-0.00093	2.39454	-0.00051	-0.00225
0.00239	-0.00134	0.59056	0.00042	-0.00023	2.01320	0.00101	-0.00057
0.00456	-0.00336	0.49313	0.00080	-0.00059	1.68109	0.00194	-0.00143
0.00617	0.00073	0.43500	0.00108	0.00013	1.48290	0.00262	0.00031
0.00626	-0.00133	0.40879	0.00110	-0.00023	1.39355	0.00266	-0.00057
0.00631	-0.00002	0.42241	0.00111	0.00000	1.43999	0.00268	-0.00001
0.00500	0.00211	0.48075	0.00088	0.00037	1.63887	0.00213	0.00090
0.00241	0.00237	0.57426	0.00042	0.00042	1.95762	0.00102	0.00101
-0.00028	0.00829	0.68655	-0.00005	0.00145	2.34045	-0.00012	0.00352
-0.00324	0.00972	0.79386	-0.00057	0.00170	2.70624	-0.00138	0.00413
-0.00627	0.00100	0.87449	-0.00110	0.00017	2.98111	-0.00266	0.00042
-0.00740	-0.00508	0.91454	-0.00130	-0.00089	3.11764	-0.00314	-0.00216
-0.00738	0.00174	0.90659	-0.00129	0.00030	3.09055	-0.00313	0.00074
-0.00461	0.00103	0.85673	-0.00081	0.00018	2.92057	-0.00196	0.00044
-0.00295	-0.00449	0.76633	-0.00052	-0.00079	2.61239	-0.00126	-0.00191
0.00012	-0.01188	0.65380	0.00002	-0.00208	2.22878	0.00005	-0.00505
0.00357	-0.00367	0.54585	0.00063	-0.00064	1.86081	0.00152	-0.00156
0.00526	-0.00100	0.46110	0.00092	-0.00018	1.57188	0.00224	-0.00043
0.00680	-0.00190	0.41097	0.00119	-0.00033	1.40097	0.00289	-0.00081
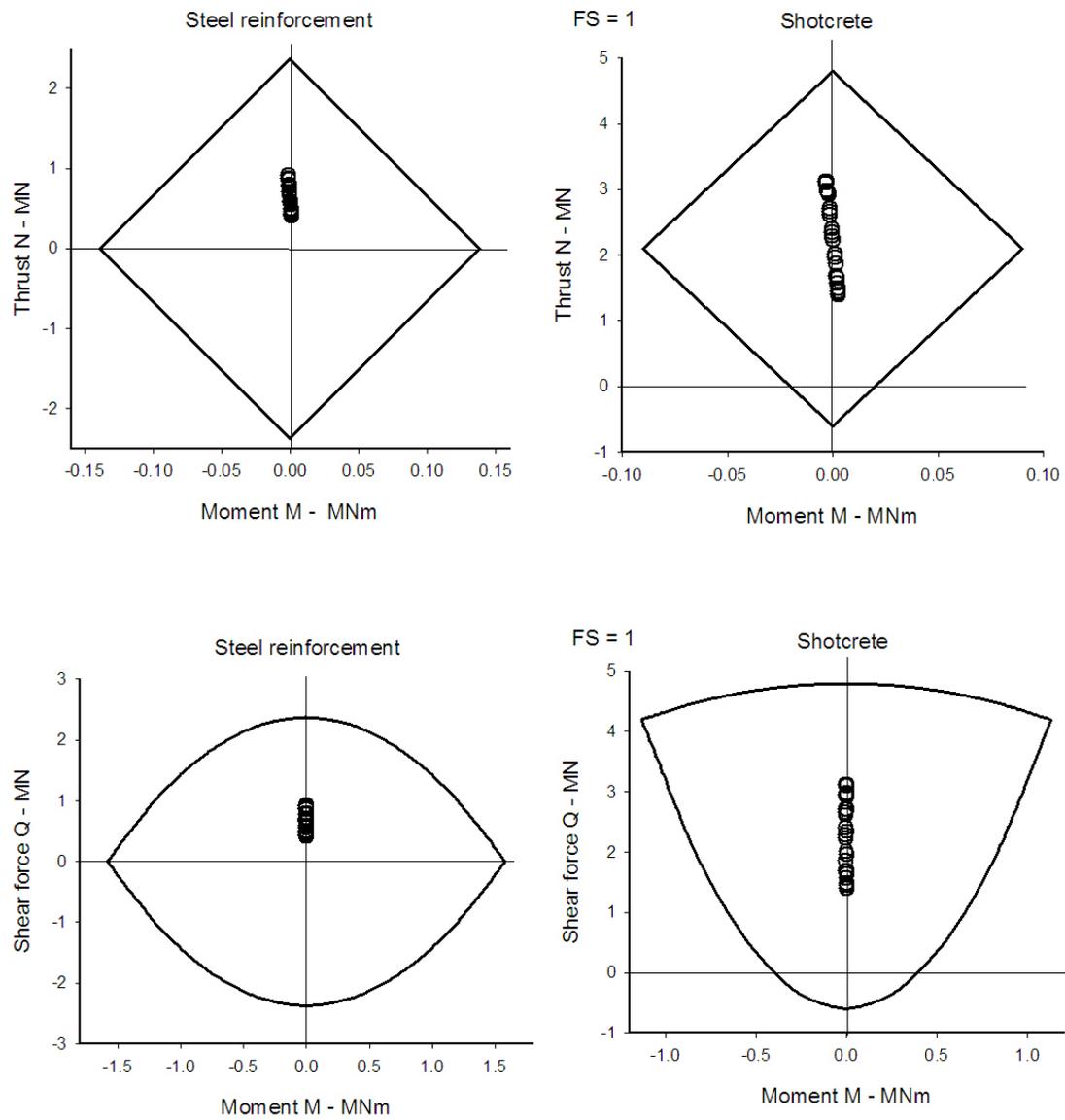
Figure A2.2. Support capacity diagrams and induced lining forces for the example described above.